A DEPTH-AVERAGED MODEL FOR GRANULAR FLOW CONSISTENT WITH THE INCOMPRESSIBLE $\mu(I)$ RHEOLOGY

Emile Deleage, Gaël Loïc Richard

A DEPTH-AVERAGED MODEL FOR GRANULAR FLOW CONSISTENT WITH THE INCOMPRESSIBLE $\mu(I)$ RHEOLOGY

ÉMILE DELÉAGE[1,2] AND GAËL L. RICHARD[2]

Abstract. We derive a depth-averaged model consistent with the $\mu(I)$ rheology for an incompressible granular flow down an inclined plane. The first two variables of the model are the depth and the depth-averaged velocity. The shear is also taken into account via a third variable called enstrophy. The obtained system is a hyperbolic system of conservation laws, with an additional equation for the energy. The system is derived from an asymptotic expansion of the flow variables in powers of the shallow-water parameter. This method ensures that the model is fully consistent with the rheology. The velocity profile is a Bagnold profile at leading order and the first-order correction to this profile can be calculated for flows that are not steady uniform. The first-order correction to the classical granular friction law is also consistently written. As a consequence, the instability threshold of the steady uniform flow is the same for the depth-averaged model and for the governing equations. In addition, a higher-order version that contains diffusive terms is also presented. The spatial growth rate, the phase velocity and the cutoff frequency of the version with diffusion are in good agreement with the experimental data and with the theoretical predictions for the rheology. The mathematical structure of the equations enables to use well-known and stable numerical solvers. Numerical simulations of granular roll waves are presented. The model has the same limitations as the $\mu(I)$ rheology, in particular for the solid/ liquid and liquid/gas transitions, and needs therefore a regularization for these transitions.

1. Introduction

The concept of granular fluid can be used in order to model the flow of a large quantity of solid particles (see Andreotti et al. (2013)). In dense regimes, the particles tend to stay in contact with each other and a macroscopic behaviour can be observed. This kind of flow can be found in many geophysical contexts, for which, in the presence of topography, the flow is driven by gravity. Two examples are landslides or dry snow avalanches. Modelling the flow of granular media with a good accuracy is thus of crucial importance in a large range of applications.

Granular flows exhibit complex behaviours that are distinct from more "classical" flows. In the context of flow down an inclined plane, a way to model these particular aspects is to use an adequate friction law. Granular friction laws were first introduced at the depth-averaged level. A first model was made in 1989 by Savage and Hutter (1989). More recently, an empirical approach was used by Pouliquen (1999) and refined by Pouliquen and Forterre (2002) to derive a friction law based on experimental observations, still at the depth-averaged level. In this law, the friction coefficient μ is a function of the dimensionless parameter I, called

Date: August 7, 2024.

inertial number. The inertial number is interpreted as a ratio between two time-scales related to the microscopic structure of the granular media (GDR MiDi, 2004). This $\mu(I)$ rheology was then generalized into a constitutive law at the bulk level, for two-dimensional (2D) flows (GDR MiDi, 2004; Pouliquen et al., 2005; Jop et al., 2005) and three-dimensional (3D) flows (Jop et al., 2006; Forterre, 2006).

For numerical applications, depth-averaged models present the advantage of a reduced computation time. Various depth-averaged models have been derived, for instance by Pouliquen and Forterre (2002), Forterre and Pouliquen (2003), Forterre (2006), Gray and Edwards (2014). We also mention the work by Mangeney-Castelnau et al. (2003), Mangeney-Castelnau et al. (2005) and Mangeney et al. (2007), for numerical simulations of such depth-averaged models. In the case of thin layers, depth-averaged models can be derived by introducing a small parameter ε, which is a ratio between a vertical and a horizontal length scale, and by using an asymptotic method with a systematic expansion of the equations as power series of the parameter ε. The leading order, or zeroth order in ε, governs the steady uniform flows. For flows that are not steady uniform, it is important to ensure consistency up to the first order in ε. This method was already used to derive consistent depth-averaged models for Newtonian fluids (Ruyer-Quil and Manneville, 2000; Richard et al., 2016) and viscoplastic flows (Denisenko et al., 2023), but no depth-averaged model of dense granular flow consistent with the incompressible $\mu(I)$ rheology has been derived. As a consequence, the instability threshold of steady uniform flows of the existing models is different from the theoretical one that was obtained by Forterre (2006) with the $\mu(I)$ rheology.

The formation of roll waves for dense granular flows was experimentally observed by Forterre and Pouliquen (2003) above a critical Froude number. They also measured the phase velocity and the spatial growth rate. They showed the existence of a cut-off frequency, above which the instability disappears. This cut-off frequency does not appear in models that only take into account friction effects. For such models, the roll wave instability occurs above a critical Froude number for a perturbation with an arbitrarily large frequency, whereas the experiments show that there is no instability above the cut-off frequency. However, this cut-off frequency was successfully obtained with more complete models that also include diffusive effects, which are of second order in ε. This is the case of the models of Forterre (2006) and Gray and Edwards (2014) for instance. Although the expressions of the diffusive terms proposed in these models are different from each other, they both predict a cut-off frequency in agreement with the experimental data of Forterre and Pouliquen (2003), and they also predict efficiently the spatial growth rate. Hence the inclusion of diffusion is important for modelling roll-waves in dense granular flows.

If a no-slip condition is assumed at the bottom, the flow is strongly sheared and shear effects cannot be consistently neglected in the depth-averaged model. A first approach that has been used by Forterre and Pouliquen (2003) and Gray and Edwards (2014) is to introduce a parameter α, called shape factor, which depends on the velocity profile. For a sheared flow, the shape factor is always greater than 1. In the case of steady and uniform granular flows, the velocity profile is a Bagnold profile (Andreotti et al., 2013) and the shape factor is equal to $5/4$. However, if a shape factor $\alpha \neq 1$ is used in a shallow-water model, there is no energy balance equation for the system. It is usually better to use $\alpha = 1$, thus

loosing the consistency for a sheared flow. Another approach, which was initiated by Teshukov (2007) and developed by Richard and Gavrilyuk (2012), is to take the shear into account with an additional variable, which was called enstrophy because it is related to the square of the vorticity. The depth-averaged model is thus a system of three variables. The first two variables, which are the depth of the flow and the depth-averaged velocity, are the usual variables for shallow-water equations. The third variable is the enstrophy. In one dimension (1D), the obtained model is a hyperbolic system of conservation laws analogous to the compressible Euler equations. This enables to use well-known reliable and stable numerical schemes. This approach is quite general and has been used to derive depth-averaged models in various contexts, see for instance Richard et al. (2016), Denisenko et al. (2023), Richard (2024).

In this paper, we derive a depth-averaged model from the bulk $\mu(I)$ rheology. Our first goal in this work is to obtain a fully consistent model, up to order 1 in ε. The paper is organized as follows: in §2, we present the equations that govern the motion of the granular medium, as well as their dimensionless form in the long-wave asymptotic. In §3, we derive explicitly the asymptotic expansions at orders 0 and 1 in ε. In §4, the depth-averaged model is derived. The model is analysed in §5 and is compared with experimental data of Forterre and Pouliquen (2003). An extended version of the model, that takes into account diffusive effects, is given in §5.4. The need for a regularized model is explained in §6.

2. Governing equations

2.1. **Constitutive equations.** We study the flow of a granular fluid, which is described by its density ρ and its velocity $\boldsymbol{v}$. We assume that the fluid is made of solid particles. Hence the density is proportional to ϕ the volume fraction of the beads and is written

$$\rho = \rho_p \phi, \tag{2.1}$$

where the constant ρ_p is the density of the beads. We also suppose that the volume fraction ϕ is constant, which implies that the flow is incompressible. We assume that the fluid is flowing down an inclined plane that makes an angle θ with the horizontal. The motion of the fluid is described by the Navier-Stokes equations, which read in the incompressible case with constant density

$$\begin{aligned} \frac{\partial \rho \boldsymbol{v}}{\partial t} + \mathbf{div}\,(\rho \boldsymbol{v} \otimes \boldsymbol{v}) &= \mathbf{div}\,\boldsymbol{\sigma} + \rho \boldsymbol{g}, \\ \operatorname{div} \boldsymbol{v} &= 0, \\ \phi &= \phi_c \text{ constant}. \end{aligned} \tag{2.2}$$

The second order tensor $\boldsymbol{\sigma}$ is called the Cauchy stress tensor and can be written

$$\boldsymbol{\sigma} = -p\mathbf{I}_d + \boldsymbol{\tau}, \tag{2.3}$$

where $\mathbf{I_d}$ is the identity tensor. The quantity p is the pressure and $\boldsymbol{\tau}$ is the deviatoric stress tensor. It is given by the constitutive law

$$\boldsymbol{\tau} = \eta_e \dot{\boldsymbol{\gamma}}, \tag{2.4}$$

where

$$\dot{\boldsymbol{\gamma}} = \mathbf{grad}\,\boldsymbol{v} + (\mathbf{grad}\,\boldsymbol{v})^{\mathrm{T}} \tag{2.5}$$

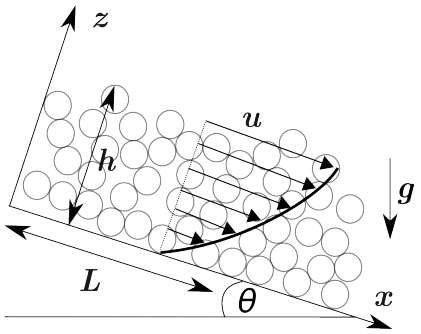

FIGURE 1. Definition sketch.

is the strain-rate tensor and η_e is an effective viscosity. In the isotropic case, η_e is a scalar. In order to define the effective viscosity, we introduce the inertial number I, which is a dimensionless parameter given by the relation (GDR MiDi, 2004)

$$I = \frac{|\dot{\boldsymbol{\gamma}}|d}{\sqrt{p/\rho_p}}. \tag{2.6}$$

The quantity d is the diameter of a bead, and $|\dot{\boldsymbol{\gamma}}|$ is the norm of the second order tensor $\dot{\boldsymbol{\gamma}}$, defined by

$$|\dot{\boldsymbol{\gamma}}| = \sqrt{\frac{\dot{\boldsymbol{\gamma}} : \dot{\boldsymbol{\gamma}}}{2}}. \tag{2.7}$$

We also introduce the friction coefficient $\mu(I)$, which depends only on I. The dependence is experimentally determined with three constants μ_1, μ_2 and I_m as (Jop et al., 2006)

$$\mu(I) = \mu_1 + \frac{\mu_2 - \mu_1}{1 + I_m/I}. \tag{2.8}$$

The two constants μ_1 and μ_2 are limit cases: the value μ_2 is the maximal value of $\mu(I)$, obtained when $I \to \infty$, the value μ_1 is the minimal value, obtained when $I = 0$, and the granular fluid only flows when $|\tau| > \mu_1 p$. Note that this relation can be inverted to write

$$I = I_m \frac{\mu - \mu_1}{\mu_2 - \mu} \tag{2.9}$$

The expression of the effective viscosity is then

$$\eta_e = \mu(I)\frac{p}{|\dot{\boldsymbol{\gamma}}|}. \tag{2.10}$$

We denote by z the coordinate in the direction normal to the inclined plane and by x the coordinate in the direction parallel to the inclined plane (see Figure 1). The components of the velocity $\boldsymbol{v}$ are u and w in the x-direction and in the z-direction respectively.

The system (2.2) admits an energy balance equation. The mechanical energy density E of the fluid is equal to the sum of the kinetic energy density and the gravitational potential energy density:

$$E = \frac{1}{2}\rho|\boldsymbol{v}|^2 - \rho g x \sin\theta + \rho g z \cos\theta. \tag{2.11}$$

The energy balance equation is then

$$\frac{\partial E}{\partial t} + \operatorname{div}\left(E\boldsymbol{v}\right) = \operatorname{div}\left(\boldsymbol{\sigma}\cdot\boldsymbol{v}\right) - \frac{\boldsymbol{\sigma}:\dot{\boldsymbol{\gamma}}}{2}. \tag{2.12}$$

Using the incompressibility condition, Equation (2.12) can also be written

$$\frac{\partial E}{\partial t} + \operatorname{div}\left[\left(E+p\right)\boldsymbol{v}\right] = \operatorname{div}\left(\boldsymbol{\tau}\cdot\boldsymbol{v}\right) - \frac{\boldsymbol{\tau}:\dot{\boldsymbol{\gamma}}}{2}. \tag{2.13}$$

The granular fluid is assumed to be delimited downwards by the inclined plane at $z=0$, and a free surface upwards at $z=h$. The field h is a function of (t,x). For any field f depending on the variable z, we write $f(0) := f|_{z=0}$, and $f(h) := f|_{z=h}$. We denote by $\boldsymbol{n}(t,x)$ the unit vector normal to the free surface and pointing outward the flow. It is given by

$$\boldsymbol{n} = \frac{1}{\sqrt{1+|\partial h/\partial x|^2}}\left(-\frac{\partial h}{\partial x}, 1\right)^{\mathrm{T}}. \tag{2.14}$$

We can now define the boundary conditions satisfied by the velocity:

– At $z=0$, we assume a non-penetration condition given by

$$w(0) = 0, \tag{2.15}$$

as well as a no-slip condition, given by

$$u(0) = 0. \tag{2.16}$$

– At $z=h$, the velocity drives the evolution of the free surface via the kinematic boundary condition

$$\frac{\partial h}{\partial t} + u(h)\frac{\partial h}{\partial x} = w(h). \tag{2.17}$$

The dynamic boundary condition states that the normal stresses are continuous across the free surface. The normal stress above the free surface is given by the atmospheric pressure p_{atm}. Without loss of generality, this constant can be taken equal to zero. This leads to the equation

$$\boldsymbol{\sigma}(h)\cdot\boldsymbol{n} = 0, \tag{2.18}$$

which expands as

$$\begin{cases} \tau_{xz}(h) + p(h)\dfrac{\partial h}{\partial x} - \tau_{xx}(h)\dfrac{\partial h}{\partial x} = 0, & \text{(2.19a)} \\ \tau_{zz}(h) - p(h) - \tau_{xz}(h)\dfrac{\partial h}{\partial x} = 0. & \text{(2.19b)} \end{cases}$$

2.2. **Dimensionless form of the equations.** We write here all equations in a non-dimensional form. In order to do so, we denote, for any field f, a corresponding dimensionless field by $\tilde{f}$.

We assume here that the flow occurs at a typical horizontal scale L_0, and a typical vertical scale h_0, such that $\varepsilon = h_0/L_0 \ll 1$ is a small parameter. We also assume that the horizontal velocity is of order u_0, such that the Froude number

$$F = \frac{u_0}{\sqrt{g h_0}} \tag{2.20}$$

is of $O(1)$, as it is the case for instance in the experiments performed by Pouliquen (1999) and Forterre and Pouliquen (2003). We introduce the following dimensionless variables:

$$\tilde{x} = \frac{x}{L_0}, \quad \tilde{z} = \frac{z}{h_0}, \quad \tilde{h} = \frac{h}{h_0}. \tag{2.21}$$

The time and velocity are scaled according to the usual shallow-water scaling as

$$\tilde{t} = t\frac{u_0}{L_0}, \quad \tilde{u} = \frac{u}{u_0}, \quad \tilde{w} = \frac{w}{\varepsilon u_0}, \tag{2.22}$$

The dimensionless pressure, density and size of the beads are found by

$$\tilde{p} = \frac{p}{\rho_p g h_0}, \quad \tilde{\rho} = \frac{\rho}{\rho_p} = \phi, \quad \tilde{d} = \frac{d}{h_0}. \tag{2.23}$$

We also scale the deviatoric stress tensor as

$$\tilde{\tau}_{xx} = \frac{\tau_{xx}}{\varepsilon \rho_p g h_0}, \quad \tilde{\tau}_{zz} = \frac{\tau_{zz}}{\varepsilon \rho_p g h_0}, \quad \tilde{\tau}_{xz} = \frac{\tau_{xz}}{\rho_p g h_0} \tag{2.24}$$

and the strain-rate tensor and energy as

$$|\tilde{\dot{\boldsymbol{\gamma}}}| = |\dot{\boldsymbol{\gamma}}|\frac{h_0}{u_0}, \qquad \tilde{E} = \frac{E}{\rho_p u_0^2}. \tag{2.25}$$

We obtain

$$\tilde{\tau}_{xx} = 2\mu(I)\frac{\tilde{p}}{|\tilde{\dot{\boldsymbol{\gamma}}}|}\frac{\partial \tilde{u}}{\partial \tilde{x}}, \quad \tilde{\tau}_{zz} = 2\mu(I)\frac{\tilde{p}}{|\tilde{\dot{\boldsymbol{\gamma}}}|}\frac{\partial \tilde{w}}{\partial \tilde{z}}, \quad \tilde{\tau}_{xz} = \mu(I)\frac{\tilde{p}}{|\tilde{\dot{\boldsymbol{\gamma}}}|}\left(\frac{\partial \tilde{u}}{\partial \tilde{z}} + \varepsilon^2\frac{\partial \tilde{w}}{\partial \tilde{x}}\right). \tag{2.26}$$

with

$$I = \frac{|\tilde{\dot{\boldsymbol{\gamma}}}|\tilde{d}}{\sqrt{\tilde{p}}}F, \tag{2.27}$$

and

$$|\tilde{\dot{\boldsymbol{\gamma}}}| = \left[\left(\frac{\partial \tilde{u}}{\partial \tilde{z}} + \varepsilon^2\frac{\partial \tilde{w}}{\partial \tilde{x}}\right)^2 + 2\varepsilon^2\left(\frac{\partial \tilde{u}}{\partial \tilde{x}}\right)^2 + 2\varepsilon^2\left(\frac{\partial \tilde{w}}{\partial \tilde{z}}\right)^2\right]^{1/2}. \tag{2.28}$$

The dimensionless energy reads

$$\tilde{E} = \frac{1}{2}\phi\left(\tilde{u}^2 + \varepsilon^2\tilde{w}^2\right) - \frac{\phi\sin\theta}{\varepsilon F^2}\tilde{x} + \frac{\phi\cos\theta}{F^2}\tilde{z}. \tag{2.29}$$

The divergence-free condition stays true for the new variables:

$$\frac{\partial \tilde{u}}{\partial \tilde{x}} + \frac{\partial \tilde{w}}{\partial \tilde{z}} = 0. \tag{2.30}$$

The momentum equation in the x-direction becomes

$$\frac{\partial \phi\tilde{u}}{\partial \tilde{t}} + \frac{\partial \phi\tilde{u}^2}{\partial \tilde{x}} + \frac{\partial \phi\tilde{u}\tilde{w}}{\partial \tilde{z}} = \frac{\phi\sin\theta}{\varepsilon F^2} - \frac{1}{F^2}\frac{\partial \tilde{p}}{\partial \tilde{x}} + \frac{\varepsilon}{F^2}\frac{\partial \tilde{\tau}_{xx}}{\partial \tilde{x}} + \frac{1}{\varepsilon F^2}\frac{\partial \tilde{\tau}_{xz}}{\partial \tilde{z}}. \tag{2.31}$$

In the z-direction, we obtain

$$\varepsilon^2\left(\frac{\partial \phi\tilde{w}}{\partial \tilde{t}} + \frac{\partial \phi\tilde{u}\tilde{w}}{\partial \tilde{x}} + \frac{\partial \phi\tilde{w}^2}{\partial \tilde{z}}\right) = -\frac{\phi\cos\theta}{F^2} - \frac{1}{F^2}\frac{\partial \tilde{p}}{\partial \tilde{z}} + \frac{\varepsilon}{F^2}\frac{\partial \tilde{\tau}_{xz}}{\partial \tilde{x}} + \frac{\varepsilon}{F^2}\frac{\partial \tilde{\tau}_{zz}}{\partial \tilde{z}}. \tag{2.32}$$

The energy equation (2.13) gives

$$\frac{\partial \tilde{E}}{\partial \tilde{t}} + \operatorname{div}\left[\left(\tilde{E} + \frac{\tilde{p}}{F^2}\right)\tilde{\boldsymbol{v}}\right] = \frac{1}{F^2}\left[\tilde{u}\left(\varepsilon\frac{\partial \tilde{\tau}_{xx}}{\partial \tilde{x}} + \frac{1}{\varepsilon}\frac{\partial \tilde{\tau}_{xz}}{\partial \tilde{z}}\right) + \varepsilon\tilde{w}\left(\frac{\partial \tilde{\tau}_{xz}}{\partial \tilde{x}} + \frac{\partial \tilde{\tau}_{zz}}{\partial \tilde{z}}\right)\right], \tag{2.33}$$

where we denoted by $\tilde{\boldsymbol{v}}$ the dimensionless velocity field.

Finally, we can rewrite the boundary conditions. For the velocity, we obtain

$$\tilde{u}(0) = 0, \;\; \tilde{w}(0) = 0, \;\; \frac{\partial h}{\partial t} + \tilde{u}(\tilde{h})\frac{\partial \tilde{h}}{\partial \tilde{x}} = \tilde{w}(\tilde{h}). \tag{2.34}$$

Equations (2.19) become in the new variables

$$\begin{cases} \tilde{\tau}_{xz}(\tilde{h}) + \varepsilon \tilde{p}(\tilde{h})\dfrac{\partial \tilde{h}}{\partial \tilde{x}} - \varepsilon^2 \tilde{\tau}_{xx}(\tilde{h})\dfrac{\partial \tilde{h}}{\partial \tilde{x}} = 0, & \text{(2.35a)} \\ \varepsilon \tilde{\tau}_{zz}(\tilde{h}) - \tilde{p}(\tilde{h}) - \varepsilon \tilde{\tau}_{xz}(\tilde{h})\dfrac{\partial \tilde{h}}{\partial \tilde{x}} = 0. & \text{(2.35b)} \end{cases}$$

3. Asymptotic expansion up to the first order

We now make the hypothesis that every variable f of the problem admits an asymptotic expansion as

$$f = f^{(0)} + \varepsilon f^{(1)} + O(\varepsilon^2). \tag{3.1}$$

We thus write such an expansion for every dimensionless variable of the problem. Injecting these expansions into the mass conservation law (2.30), the momentum balance equations (2.31)–(2.32) and the constitutive law (2.26), taking into account the boundary conditions, we can compute explicitly all terms in the expansions up to order 1.

3.1. **Order 0.**

At leading order, we obtain from Equations (2.31), (2.32), (2.35) the following relations:

$$0 = \frac{\phi \sin\theta}{F^2} + \frac{1}{F^2}\frac{\partial \tilde{\tau}_{xz}^{(0)}}{\partial \tilde{z}}, \tag{3.2}$$

$$0 = -\frac{\phi \cos\theta}{F^2} - \frac{1}{F^2}\frac{\partial \tilde{p}^{(0)}}{\partial \tilde{z}} \tag{3.3}$$

$$0 = \tilde{\tau}_{xz}^{(0)}(\tilde{h}), \tag{3.4}$$

$$0 = \tilde{p}^{(0)}(\tilde{h}). \tag{3.5}$$

We integrate the first two equations between $\tilde{z}$ and $\tilde{h}$ using the conditions at $\tilde{z} = \tilde{h}$ to obtain

$$\tilde{\tau}_{xz}^{(0)} = \phi \sin\theta(\tilde{h} - \tilde{z}) \tag{3.6}$$

and

$$\tilde{p}^{(0)} = \phi \cos\theta(\tilde{h} - \tilde{z}). \tag{3.7}$$

The pressure is thus hydrostatic at this order. Equation (2.27) gives, after using the physical assumption that $\partial \tilde{u}^{(0)}/\partial \tilde{z} > 0$,

$$|\tilde{\dot{\boldsymbol{\gamma}}}|^{(0)} = \frac{\partial \tilde{u}^{(0)}}{\partial \tilde{z}}. \tag{3.8}$$

Equation (2.26) then gives

$$\tilde{\tau}_{xz}^{(0)} = \mu^{(0)} \tilde{p}^{(0)} \tag{3.9}$$

with $\mu^{(0)} = \mu(I^{(0)})$. We have $\mu^{(0)} = \tau_{xz}^{(0)}/p^{(0)}$. This yields

$$\mu^{(0)} = \tan\theta. \tag{3.10}$$

At order 0, the friction coefficient has the same expression as in the case of a steady uniform flow. The expression of the inertial number at order 0 is

$$I^{(0)} = \frac{\tan\theta - \mu_1}{\mu_2 - \tan\theta} I_m \tag{3.11}$$

by (2.9). It follows from (3.8) and (2.27) that

$$\frac{\partial \tilde{u}^{(0)}}{\partial \tilde{z}} = \frac{I^{(0)}}{\tilde{d}F}\sqrt{\phi\cos\theta(\tilde{h}-\tilde{z})}, \tag{3.12}$$

that we integrate using (2.34) to obtain

$$\tilde{u}^{(0)} = \frac{2\tilde{A}}{3}\left[\tilde{h}^{3/2} - \left(\tilde{h}-\tilde{z}\right)^{3/2}\right], \tag{3.13}$$

where we defined

$$\tilde{A} = \frac{I^{(0)}}{\tilde{d}F}\sqrt{\phi\cos\theta}, \qquad \text{and} \qquad A = \frac{I^{(0)}\sqrt{\phi g\cos\theta}}{d}. \tag{3.14}$$

At order 0, the velocity profile in the z-direction is a Bagnold profile, as expected from the $\mu(I)$-rheology. At this order, the depth-averaged velocity is $\tilde{U}^{(0)} = 2\tilde{A}\tilde{h}^{3/2}/5$. If the characteristic velocity u_0 and the vertical scale h_0 are taken equal respectively to the depth-averaged velocity and depth of the steady uniform flow, then $\tilde{A} = 5/2$.

We deduce, using (2.30) ,

$$\frac{\partial \tilde{w}^{(0)}}{\partial \tilde{z}} = \tilde{A}\left[\left(\tilde{h}-\tilde{z}\right)^{1/2} - \tilde{h}^{1/2}\right]\frac{\partial \tilde{h}}{\partial \tilde{x}}, \tag{3.15}$$

which is integrated as

$$\tilde{w}^{(0)} = \tilde{A}\left[\frac{2}{3}\tilde{h}^{3/2} - \frac{2}{3}\left(\tilde{h}-\tilde{z}\right)^{3/2} - \tilde{z}\tilde{h}^{1/2}\right]\frac{\partial \tilde{h}}{\partial \tilde{x}}. \tag{3.16}$$

Finally, we use (2.26) to obtain

$$\tilde{\tau}_{xx}^{(0)} = -\tilde{\tau}_{zz}^{(0)} = 2\phi\sin\theta\left[\tilde{h}^{1/2}\left(\tilde{h}-\tilde{z}\right)^{1/2} - \tilde{h} + \tilde{z}\right]\frac{\partial \tilde{h}}{\partial \tilde{x}}. \tag{3.17}$$

3.2. **Order 1.** We now investigate Equations (2.31), (2.32) and (2.35) at the first order. At this order of accuracy, these equations become

$$\frac{\partial \tilde{u}^{(0)}}{\partial \tilde{t}} + \tilde{u}^{(0)}\frac{\partial \tilde{u}^{(0)}}{\partial \tilde{x}} + \tilde{w}^{(0)}\frac{\partial \tilde{u}^{(0)}}{\partial \tilde{z}} = -\frac{1}{\phi F^2}\frac{\partial \tilde{p}^{(0)}}{\partial \tilde{x}} + \frac{1}{\phi F^2}\frac{\partial \tilde{\tau}_{xz}^{(1)}}{\partial \tilde{z}}, \tag{3.18}$$

$$0 = -\frac{1}{F^2}\frac{\partial \tilde{p}^{(1)}}{\partial \tilde{z}} + \frac{1}{F^2}\frac{\partial \tilde{\tau}_{xz}^{(0)}}{\partial \tilde{x}} + \frac{1}{F^2}\frac{\partial \tilde{\tau}_{zz}^{(0)}}{\partial \tilde{z}} \tag{3.19}$$

$$0 = \tilde{\tau}_{xz}^{(1)}(\tilde{h}) + \tilde{p}^{(0)}(\tilde{h})\frac{\partial \tilde{h}}{\partial \tilde{x}}, \tag{3.20}$$

$$0 = \tilde{\tau}_{zz}^{(0)}(\tilde{h}) - \tilde{p}^{(1)}(\tilde{h}) - \tilde{\tau}_{xz}^{(0)}(\tilde{h})\frac{\partial \tilde{h}}{\partial \tilde{x}}. \tag{3.21}$$

In view of the values of $\tilde{\tau}_{xz}^{(0)}(\tilde{h})$, $\tilde{\tau}_{zz}^{(0)}(\tilde{h})$ and $\tilde{p}^{(0)}(\tilde{h})$ (see (3.6), (3.17) and (3.7)), we obtain from the two last equations

$$\tilde{\tau}_{xz}^{(1)}(\tilde{h}) = \tilde{p}^{(1)}(\tilde{h}) = 0. \tag{3.22}$$

We inject the values of $\tilde{u}^{(0)}$, $\tilde{w}^{(0)}$ and $\tilde{p}^{(0)}$, using Equation (2.34) to express $\partial\tilde{h}/\partial\tilde{t}$ at the leading order as $\partial\tilde{h}/\partial\tilde{t} = -\tilde{A}\tilde{h}^{3/2}\partial\tilde{h}/\partial\tilde{x}$, to obtain

$$\frac{\partial\tilde{\tau}_{xz}^{(1)}}{\partial\tilde{z}} = \phi\frac{\partial\tilde{h}}{\partial\tilde{x}}\left[\cos\theta + \frac{F^2\tilde{A}^2}{3}\left(\tilde{h}^{1/2}(\tilde{h}-\tilde{z})^{3/2} - \tilde{h}^2\right)\right]. \tag{3.23}$$

This expression is integrated between $\tilde{z}$ and $\tilde{h}$ with the boundary condition. This yields

$$\tilde{\tau}_{xz}^{(1)} = \phi\frac{\partial\tilde{h}}{\partial\tilde{x}}\left[\frac{F^2\tilde{A}^2}{3}\left((\tilde{h}-\tilde{z})\tilde{h}^2 - \frac{2}{5}\tilde{h}^{1/2}(\tilde{h}-\tilde{z})^{5/2}\right) - \cos\theta(\tilde{h}-\tilde{z})\right]. \tag{3.24}$$

We now inject the values of $\tilde{\tau}_{xz}^{(0)}$ and $\tilde{\tau}_{zz}^{(0)}$ into the second equation. We find

$$\frac{\partial\tilde{p}}{\partial\tilde{z}}^{(1)} = \phi\sin\theta\frac{\partial\tilde{h}}{\partial\tilde{x}}\left[\frac{\tilde{h}^{1/2}}{\left(\tilde{h}-\tilde{z}\right)^{1/2}} - 1\right], \tag{3.25}$$

which is integrated between $\tilde{z}$ and $\tilde{h}$ to calculate the expression of the first-order correction to the pressure as

$$\tilde{p}^{(1)} = \phi\sin\theta\frac{\partial\tilde{h}}{\partial\tilde{x}}\left[\tilde{h}-\tilde{z} - 2\tilde{h}^{1/2}\left(\tilde{h}-\tilde{z}\right)^{1/2}\right]. \tag{3.26}$$

We also obtain from (2.28)

$$\left|\tilde{\dot{\boldsymbol{\gamma}}}\right|^{(1)} = \frac{\partial\tilde{u}}{\partial\tilde{z}}^{(1)}. \tag{3.27}$$

Hence, with (2.26), we can write $\tilde{\tau}_{xz}^{(1)} = \mu(I)^{(1)}\tilde{p}^{(0)} + \mu(I)^{(0)}\tilde{p}^{(1)}$. Therefore, the first-order correction to the friction coefficient can be consistently written as $\mu^{(1)} = (\tilde{\tau}_{xz}^{(1)} - \mu^{(0)}\tilde{p}^{(1)})/\tilde{p}^{(0)}$, which leads to the expression

$$\mu^{(1)} = \frac{\partial\tilde{h}}{\partial\tilde{x}}\left[\frac{F^2\tilde{A}^2}{3\cos\theta}\left(\tilde{h}^2 - \frac{2}{5}\tilde{h}^{1/2}(\tilde{h}-\tilde{z})^{3/2}\right) - \frac{1}{\cos^2\theta} + 2\tilde{h}^{1/2}(\tilde{h}-\tilde{z})^{-1/2}\tan^2\theta\right]. \tag{3.28}$$

We now deduce the expression of the first-order correction to the inertial number, writing

$$I^{(1)} = \left.\frac{\partial I}{\partial\mu}\right|_{\mu^{(0)}}\mu^{(1)}, \tag{3.29}$$

to find

$$I^{(1)} = I_m\frac{\mu_2-\mu_1}{(\mu_2-\tan\theta)^2}\mu^{(1)}. \tag{3.30}$$

We can write

$$I^{(1)} = B\,I^{(0)}\mu^{(1)} \tag{3.31}$$

where $B = (\partial\ln I/\partial\mu)(\mu=\tan\theta)$ or

$$B = \frac{\mu_2-\mu_1}{(\mu_2-\tan\theta)(\tan\theta-\mu_1)}. \tag{3.32}$$

At first order, the expansion of (2.27) gives

$$\left|\tilde{\dot{\gamma}}\right|^{(1)} = \frac{1}{\tilde{d}F}\left(I^{(1)}\sqrt{p^{(0)}} + \frac{I^{(0)}p^{(1)}}{2\sqrt{p^{(0)}}}\right). \tag{3.33}$$

Equations (3.26), (3.31), (3.27) and (3.7) can be used to obtain

(3.34)

$$\frac{\partial \tilde{u}}{\partial \tilde{z}}^{(1)} = \tilde{A}\frac{\partial \tilde{h}}{\partial \tilde{x}}\left\{\frac{BF^2\tilde{A}^2}{3\cos\theta}\left[\tilde{h}^2\left(\tilde{h}-\tilde{z}\right)^{1/2} - \frac{2}{5}\tilde{h}^{1/2}\left(\tilde{h}-\tilde{z}\right)^2\right] - \frac{B\left(\tilde{h}-\tilde{z}\right)^{1/2}}{\cos^2\theta}\right.$$
$$\left. + 2B\tilde{h}^{1/2}\tan^2\theta + \frac{\tan\theta}{2}\left(\tilde{h}-\tilde{z}\right)^{1/2} - \tilde{h}^{1/2}\tan\theta\right\}.$$

The integration of this expression leads to

(3.35)

$$u^{(1)} = \tilde{A}\frac{\partial \tilde{h}}{\partial \tilde{x}}\left\{\frac{2BF^2\tilde{A}^2}{9\cos\theta}\left[\tilde{h}^2\left(\tilde{h}^{3/2} - \left(\tilde{h}-\tilde{z}\right)^{3/2}\right) - \frac{\tilde{h}^{1/2}}{5}\left(\tilde{h}^3 - \left(\tilde{h}-\tilde{z}\right)^3\right)\right]\right.$$
$$\left. + \left(\tan\theta - \frac{2B}{\cos^2\theta}\right)\frac{\tilde{h}^{3/2} - \left(\tilde{h}-\tilde{z}\right)^{3/2}}{3} + \left(2B\tan\theta - 1\right)\tilde{h}^{1/2}\tilde{z}\tan\theta\right\},$$

which is the consistent first-order correction to the Bagnold velocity profile.

4. Derivation of the depth-averaged equations

4.1. **Averaged variables.** We now define depth-averaged variables, and give an explicit asymptotic expansion of these variables up to the first order.The average over the depth of any quantity X is defined as

$$\langle X\rangle = \frac{1}{h}\int_0^h X \,\mathrm{d}z. \tag{4.1}$$

To lighten the notation, the depth-averaged velocity is denoted by $U = \langle u\rangle$. The average velocity $\tilde{U}$ admits an asymptotic expansion given by

$$\tilde{U} = \tilde{U}^{(0)} + \varepsilon\tilde{U}^{(1)} + O(\varepsilon^2), \tag{4.2}$$

where, by (3.13),

$$\tilde{U}^{(0)} = \frac{2}{5}\tilde{A}\tilde{h}^{3/2}, \tag{4.3}$$

and, from (3.35), after some computations,

$$\tilde{U}^{(1)} = \frac{\tilde{A}B}{10}\frac{\partial \tilde{h}}{\partial \tilde{x}}\left[\frac{F^2\tilde{A}^2}{\cos\theta}\tilde{h}^{7/2} + \left(6\tan^2\theta - 4 - \frac{3\tan\theta}{B}\right)\tilde{h}^{3/2}\right]. \tag{4.4}$$

Note that the first-order correction $U^{(1)}$ can be written

$$\tilde{U}^{(1)} = \frac{\tilde{U}-\tilde{U}^{(0)}}{\varepsilon} + O(\varepsilon) = \frac{1}{\varepsilon}\left(\tilde{U} - \frac{2}{5}\tilde{A}\tilde{h}^{3/2}\right) + O(\varepsilon), \tag{4.5}$$

To simplify the notations, we define $C = \tan\theta(2\tan\theta - 1/B)$, i.e.

$$C = \tan^2\theta + \tan\theta\left[\frac{(\tan\theta - \mu_1)^2}{\mu_2 - \mu_1} + \mu_1\right]. \tag{4.6}$$

Note that $C = C(\theta)$ is a positive increasing function of θ. It takes values in the interval $[2\mu_1^2, 2\mu_2^2]$ if $\theta \in [\arctan\mu_1, \arctan\mu_2]$. With this new notation, the function $\tilde{U}^{(1)}$ can be written:

$$\tilde{U}^{(1)} = \frac{\tilde{A}B}{10}\frac{\partial\tilde{h}}{\partial\tilde{x}}\left[\frac{F^2\tilde{A}^2}{\cos\theta}\tilde{h}^{7/2} + (3C-4)\tilde{h}^{3/2}\right]. \tag{4.7}$$

We also define a quantity, called enstrophy, as $\psi = \left\langle (u-U)^2\right\rangle / h^2$. The enstrophy takes into account shear effects. It is zero for a velocity constant in the depth and positive otherwise. The enstrophy is scaled as $\psi = \tilde{\psi}u_0^2/h_0^2$. With this definition, $\tilde{h}\left\langle \tilde{u}^2\right\rangle = \tilde{h}\tilde{U}^2 + \tilde{h}^3\tilde{\psi}$. Similarly, $\tilde{\psi}$ expands as $\tilde{\psi} = \tilde{\psi}^{(0)} + \varepsilon\tilde{\psi}^{(1)} + O(\varepsilon^2)$, where

$$\tilde{\psi}^{(0)} = \frac{\tilde{A}^2\tilde{h}}{25} \tag{4.8}$$

is the consistent expression of the enstrophy for a Bagnold profile, and

$$\tilde{\psi}^{(1)} = \frac{\tilde{A}^2B}{25}\frac{\partial\tilde{h}}{\partial\tilde{x}}\left[\frac{6F^2\tilde{A}^2}{11\cos\theta}\tilde{h}^3 + \left(\frac{13}{7}C - 2\right)\tilde{h}\right]. \tag{4.9}$$

At leading order, the enstrophy and the depth-averaged velocity satisfy the relation

$$\tilde{\psi}^{(0)} = \frac{(\tilde{U}^{(0)})^2}{4\tilde{h}^2}. \tag{4.10}$$

Note that this expression gives at leading order $h\langle(u^{(0)})^2\rangle = (5/4)h(U^{(0)})^2$. This is consistent with the shape factor 5/4 which is obtained for a Bagnold velocity profile. However, using the additional quantity enstrophy and a three-equation model instead of a shape factor and a two-equation model modifies and improves the mathematical structure of the model. In particular, a three-equation model admits an energy balance equation, which is not the case for a two-equation model with a shape factor different from 1.

The relation (4.10) leads to the expansion

$$\tilde{\psi} - \frac{\tilde{U}^2}{4\tilde{h}^2} = \varepsilon\left(\tilde{\psi}^{(1)} - \frac{\tilde{A}\tilde{U}^{(1)}}{5\tilde{h}^{1/2}}\right) + O(\varepsilon^2). \tag{4.11}$$

The leading term of (4.11) can be computed with Equations (4.9) and (4.7). We obtain

$$\tilde{\psi}^{(1)} - \frac{\tilde{A}\tilde{U}^{(1)}}{5\tilde{h}^{1/2}} = \frac{\tilde{A}^2B}{10}\frac{\partial\tilde{h}}{\partial\tilde{x}}\left(\frac{F^2\tilde{A}^2}{55\cos\theta}\tilde{h}^3 + \frac{C}{7}\tilde{h}\right). \tag{4.12}$$

This expression is useful to write consistently a relaxation term for the enstrophy.

4.2. **Depth-averaged mass and momentum equations.** We now want to derive evolution equations for the depth-averaged variables. We first integrate the divergence free condition (2.30) between 0 and $\tilde{h}$. Using the kinematic boundary condition (2.34), we obtain the depth-averaged mass conservation equation

$$\frac{\partial\tilde{h}}{\partial\tilde{t}} + \frac{\partial\tilde{h}\tilde{U}}{\partial\tilde{x}} = 0. \tag{4.13}$$

In order to derive an equation for $\tilde{U}$, we integrate (2.31) between 0 and $\tilde{h}$ using the boundary condition (2.34). This leads to a preliminary expression of the depth-averaged momentum balance equation

(4.14)
$$\frac{\partial \tilde{h}\tilde{U}}{\partial \tilde{t}} + \frac{\partial}{\partial \tilde{x}}\left(\tilde{h}\tilde{U}^2 + \tilde{h}^3\tilde{\psi} + \frac{1}{\phi F^2}\int_0^{\tilde{h}} \tilde{p}\mathrm{d}\tilde{z}\right) = \frac{1}{\varepsilon\phi F^2}\left(\phi \sin\theta \tilde{h} - \tilde{\tau}_{xz}(0)\right) + O(\varepsilon).$$

We first compute the integral of the pressure $\tilde{p}$. By using the expression (3.7) of $\tilde{p}^{(0)}$, we obtain

$$\int_0^{\tilde{h}} \tilde{p}\mathrm{d}\tilde{z} = \int_0^{\tilde{h}} \tilde{p}^{(0)}\mathrm{d}\tilde{z} + O(\varepsilon) = \frac{\phi\tilde{h}^2\cos\theta}{2} + O(\varepsilon). \tag{4.15}$$

Equation (4.14) thus yields

$$\frac{\partial \tilde{h}\tilde{U}}{\partial \tilde{t}} + \frac{\partial}{\partial \tilde{x}}\left(\tilde{h}\tilde{U}^2 + \tilde{h}^3\tilde{\psi} + \frac{\tilde{h}^2\cos\theta}{2F^2}\right) = \frac{1}{\varepsilon\phi F^2}\left(\phi \sin\theta \tilde{h} - \tilde{\tau}_{xz}(0)\right) + O(\varepsilon). \tag{4.16}$$

We now need to find an expression for the basal friction $\tilde{\tau}_{xz}(0)$. The basal friction for a granular flow can be written $\tilde{\tau}_{xz}(0) = \mu_b\phi\tilde{h}\cos\theta$ (Andreotti et al., 2013) where

$$\mu_b = \mu_1 + \frac{\mu_2 - \mu_1}{I_m\dfrac{2\tilde{h}^{3/2}\sqrt{\phi\cos\theta}}{5\tilde{d}F\tilde{U}} + 1}. \tag{4.17}$$

This expression can be written

$$\mu_b = \mu_1 + \frac{\mu_2 - \mu_1}{\dfrac{I_m}{I^{(0)}}\dfrac{\tilde{U}^{(0)}}{\tilde{U}} + 1} \tag{4.18}$$

which means that $\mu_b = \mu(I = I^{(0)}\tilde{U}/\tilde{U}^{(0)})$ such that $\mu_b^{(0)} = \mu^{(0)}$. This friction law is thus consistent at order 0 with the $\mu(I)$ rheology, and it was successfully used in several depth-averaged models. However, whereas $\tilde{\tau}_{xz}^{(0)}(0) = \mu_b^{(0)}\phi\tilde{h}\cos\theta$, it is important to stress that this relation is not satisfied at order 1 (i.e. $\tilde{\tau}_{xz}^{(1)}(0) \neq \mu_b^{(1)}\phi\tilde{h}\cos\theta$), which implies that this friction law is not consistent at order 1 with the rheology. The expansion of $\mu_b = \mu(I = I^{(0)}\tilde{U}/\tilde{U}^{(0)})$ gives

$$\mu_b = \mu^{(0)} + \varepsilon\left.\frac{\partial\mu}{\partial I}\right|_{I^{(0)}}\frac{I^{(0)}}{\tilde{U}^{(0)}}\tilde{U}^{(1)} + O(\varepsilon^2) \tag{4.19}$$

which can be written as

$$\mu_b = \mu^{(0)} + \varepsilon\frac{\tilde{U}^{(1)}}{B\tilde{U}^{(0)}} + O(\varepsilon^2). \tag{4.20}$$

Using Equations (3.6), (3.7) and (3.24), the shear stress at the bottom can be written

$$\tilde{\tau}_{xz}(0) = \mu^{(0)}\phi\tilde{h}\cos\theta + \varepsilon\phi\frac{\partial\tilde{h}}{\partial\tilde{x}}\left(\frac{F^2\tilde{A}^2}{5}\tilde{h}^3 - \tilde{h}\cos\theta\right) + O(\varepsilon^2). \tag{4.21}$$

Subtracting $\mu_b\phi\tilde{h}\cos\theta$ from $\tilde{\tau}_{xz}(0)$ leads to the expression of the first-order correction to the friction law

$$\tilde{\tau}_{xz}(0) - \mu_b\phi\tilde{h}\cos\theta = \varepsilon\phi R\cos\theta + O(\varepsilon^2), \tag{4.22}$$

where

$$R = -\frac{\partial \tilde{h}}{\partial \tilde{x}}\left(\frac{F^2\tilde{A}^2}{20\cos\theta}\tilde{h}^3 + \frac{3C}{4}\tilde{h}\right). \tag{4.23}$$

Equation (4.16) can then be written

$$\frac{\partial \tilde{h}\tilde{U}}{\partial \tilde{t}} + \frac{\partial}{\partial \tilde{x}}\left(\tilde{h}\tilde{U}^2 + \tilde{h}^3\tilde{\psi} + \frac{\tilde{h}^2\cos\theta}{2F^2}\right) = \frac{\tilde{h}\cos\theta}{\varepsilon F^2}(\tan\theta - \mu_b) - R\frac{\cos\theta}{F^2} + O(\varepsilon). \tag{4.24}$$

In order to derive a model with a satisfactory mathematical structure, we now need to find an expression for the first-order correction to the friction law, i.e. the term $-R\cos\theta/F^2$. We choose to split R into two terms. The first term is written in the left-hand side of Equation (4.24) as a flux, and the second term is written in the right-hand side and is expressed as a relaxation term. More precisely, for any $\lambda \geq 0$, we can write consistently, using Equation (4.12)

$$\begin{aligned} -\frac{\cos\theta}{F^2}R = C\left(\frac{3}{4} - \frac{\lambda}{7}\right)\frac{\partial}{\partial \tilde{x}}\left(\frac{\tilde{h}^2\cos\theta}{2F^2}\right) + \left(\frac{5}{16} - \frac{5\lambda}{44}\right)\frac{\partial}{\partial \tilde{x}}\left(\tilde{h}^3\tilde{\psi}^{(0)}\right) \\ + \lambda\frac{10\cos\theta}{F^2\tilde{A}^2B}\left(\tilde{\psi}^{(1)} - \frac{\tilde{A}\tilde{U}^{(1)}}{5\tilde{h}^{1/2}}\right). \end{aligned} \tag{4.25}$$

The parameter λ can be freely chosen with no loss of consistency. There is thus an infinite number of consistent models, which are all equivalent in the validity domain of the asymptotic expansion, i.e. in the shallow-water approximation, but which differ outside this domain. The arguments detailed in §5 lead us to choose

$$\lambda = \frac{847(4-3C)}{20(157C+84)}. \tag{4.26}$$

We can now inject this expression of R into Equation (4.24). We obtain

$$\frac{\partial \tilde{h}\tilde{U}}{\partial \tilde{t}} + \frac{\partial}{\partial \tilde{x}}\left(\tilde{h}\tilde{U}^2 + \beta\tilde{h}^3\tilde{\psi} + K\frac{\tilde{h}^2\cos\theta}{2F^2}\right) = \frac{\cos\theta}{\varepsilon F^2}\left[\tilde{h}(\tan\theta - \mu_b) + \frac{10\lambda}{\tilde{A}^2B}\left(\tilde{\psi} - \frac{\tilde{U}^2}{4\tilde{h}^2}\right)\right] + O(\varepsilon), \tag{4.27}$$

where

$$\beta = \frac{11}{16} + \frac{5\lambda}{44}, \qquad \text{and} \qquad K = 1 - \frac{3C}{4} + \frac{\lambda C}{7}. \tag{4.28}$$

Equation (4.27) is consistent at the first order of accuracy. The first-order correction to the usual granular friction law is written partly as a relaxation term in the right-hand side and partly in the momentum flux as corrections to the hydrostatic pressure term (K) and to the enstrophy term (β). The latter term also models shearing effects in the granular flow. The structure of this equation is similar to other models with enstrophy (Denisenko et al. (2023) for example) with an effective enstrophy equal to $\beta\psi$. There is also a factor K in the hydrostatic pressure term.

4.3. **Depth-averaged energy equation.** In order to close the system of equations obtained for $\tilde{h}$ and $\tilde{U}$ in the previous section, we need to find an evolution equation

for the variable $\tilde{\psi}$. Such an equation can be obtained from the equation of energy (2.33). We first rewrite equation (2.33) as:

$$\frac{1}{2}\frac{\partial \tilde{u}^2}{\partial \tilde{t}} + \operatorname{div}\left[\left(\frac{\tilde{u}^2}{2} - \frac{\tilde{x}\sin\theta}{\varepsilon F^2} + \frac{\phi\tilde{z}\cos\theta + \tilde{p}}{\phi F^2}\right)\tilde{\boldsymbol{v}}\right] = \frac{1}{\varepsilon\phi F^2}\tilde{u}\frac{\partial \tilde{\tau}_{xz}}{\partial \tilde{z}} + O(\varepsilon). \tag{4.29}$$

The integration of Equation (4.29) between 0 and $\tilde{h}$, using the boundary conditions (2.34) and (2.35b) and the incompressibility condition (2.30), gives

$$\begin{aligned}&\frac{\partial}{\partial \tilde{t}}\left(\int_0^{\tilde{h}} \frac{\tilde{u}^2}{2}\mathrm{d}\tilde{z} + \frac{\tilde{h}^2}{2F^2}\cos\theta\right) + \frac{\partial}{\partial \tilde{x}}\int_0^{\tilde{h}}\left(\frac{\tilde{u}^3}{2} + \frac{\tilde{u}(\tilde{p}+\phi\tilde{z}\cos\theta)}{\phi F^2}\right)\mathrm{d}\tilde{z} - \frac{\tilde{h}\tilde{U}}{\varepsilon F^2}\sin\theta \\ &= \frac{1}{\varepsilon\phi F^2}\int_0^{\tilde{h}} \tilde{u}\frac{\partial \tilde{\tau}_{xz}}{\partial \tilde{z}}\mathrm{d}\tilde{z} + O(\varepsilon).\end{aligned} \tag{4.30}$$

As in the previous section, we have $h\left\langle u^2\right\rangle = hU^2 + h^3\psi$. Similarly, $h\left\langle u^3\right\rangle$ can be written as $h\left\langle u^3\right\rangle = hU^3 + 3Uh^3\psi + h\left\langle (u-U)^3\right\rangle$. In order to close the equations, we need a formula for the third-order correlation $\left\langle (u-U)^3\right\rangle$. Since we neglect second-order terms, it is consistent to replace this term by the leading term in the asymptotic expansion, which is $h\left\langle (u-U)^3\right\rangle^{(0)} = -4\tilde{A}^3\tilde{h}^{11/2}/1375$. Hence

$$\frac{\partial}{\partial \tilde{x}}\int_0^{\tilde{h}} \frac{1}{2}\left(\tilde{u}^{(0)} - \tilde{U}^{(0)}\right)^3 \mathrm{d}\tilde{z} = -\frac{\tilde{A}^3\tilde{h}^{9/2}}{125}\frac{\partial \tilde{h}}{\partial \tilde{x}}. \tag{4.31}$$

This term is written in the right-hand side of the equation in order to obtain a model with a well-posed and simple mathematical structure. Equation (3.7) shows that, at order 0, we can write

$$\tilde{p}^{(0)} + \phi\tilde{z}\cos\theta = \phi\tilde{h}\cos\theta. \tag{4.32}$$

We can use this relation to write

$$\int_0^{\tilde{h}} \frac{\tilde{u}(\tilde{p}+\tilde{z}\cos\theta)}{\phi F^2}\mathrm{d}\tilde{z} = \frac{\tilde{h}^2\tilde{U}\cos\theta}{F^2} + O(\varepsilon). \tag{4.33}$$

The technical details of the treatment of the right-hand side of Equation (4.30) are given in Appendix A. The calculations are carried out to ensure compatibility between the energy and momentum depth-averaged equations in order to obtain a well-posed mathematical structure well suited to numerical resolution.

The final version of the energy equation can be written

$$\begin{aligned}&\frac{\partial}{\partial \tilde{t}}\left(\tilde{h}\frac{\tilde{U}^2}{2} + \frac{\beta\tilde{h}^3\tilde{\psi}}{2} + K\frac{\tilde{h}^2\cos\theta}{2F^2}\right) + \frac{\partial}{\partial \tilde{x}}\left(\frac{\tilde{h}\tilde{U}^3}{2} + \frac{3\beta\tilde{h}^3\tilde{U}\tilde{\psi}}{2} + K\frac{\tilde{h}^2\tilde{U}\cos\theta}{F^2}\right) \\ &= \frac{\tilde{U}\cos\theta}{\varepsilon F^2}\left[\tilde{h}(\tan\theta - \mu_b) + \frac{\beta\tilde{\alpha}_1}{\tilde{h}^{1/2}}\left(\tilde{U} - \frac{2}{5}\tilde{A}\tilde{h}^{3/2}\right) + \left(\beta\tilde{\alpha}_2 + \frac{10\lambda}{\tilde{A}^2B}\right)\left(\tilde{\psi} - \frac{\tilde{U}^2}{4\tilde{h}^2}\right)\right] + O(\varepsilon)\end{aligned} \tag{4.34}$$

with

$$\tilde{\alpha}_1 = -\frac{33C}{2\tilde{A}B(34C+28)}, \tag{4.35}$$

and

$$\tilde{\alpha}_2 = \frac{77(9C-12)}{2\tilde{A}^2B(34C+28)}. \tag{4.36}$$

As in the momentum equation, the effective enstrophy in this energy equation is $\beta\psi$ and there is the same factor K in the pressure term and in the potential energy. The right-hand side of this energy equation includes the power of the weight and of the usual granular friction law (4.17) but there are additional relaxation terms to obtain consistency at order 1.

The evolution equation for the variable $\tilde{\psi}$ can now be derived. In order to do this, the equation of momentum (4.27) is multiplied by $\tilde{U}$ and this new equation is subtracted from the equation of energy (4.34). This leads to

$$\frac{\partial \tilde{h}\tilde{\psi}}{\partial \tilde{t}}+\frac{\partial \tilde{h}\tilde{U}\tilde{\psi}}{\partial \tilde{x}}=\frac{2\tilde{U}\cos\theta}{\varepsilon \tilde{h}^2F^2}\left[\frac{\tilde{\alpha}_1}{\tilde{h}^{1/2}}\left(\tilde{U}-\frac{2}{5}\tilde{A}\tilde{h}^{3/2}\right)+\tilde{\alpha}_2\left(\tilde{\psi}-\frac{\tilde{U}^2}{4\tilde{h}^2}\right)\right]+O(\varepsilon). \tag{4.37}$$

The evolution equation of the enstrophy is a transport equation with relaxation source terms. The relaxation term on ψ is important and usual for an enstrophy equation and the coefficient $\tilde{\alpha}_2$ must be negative for the system to be mathematically well-posed (otherwise the enstrophy diverges exponentially). This gives the condition $C < 4/3$, which is discussed below in §6. For a slope in the range $[\mu_1, \mu_2]$, this condition is automatically satisfied if $\mu_2 < \sqrt{2/3} \simeq 0.816 \simeq \tan(39.2°)$.

5. Model analysis

5.1. **Hyperbolicity.** In this section, we study some properties of the model obtained in Section 4 and formed by the mass conservation equation (4.13), the momentum balance equation (4.27) and the enstrophy equation (4.37). In dimensional form, this system reads

(5.1)
$$\begin{cases}\dfrac{\partial h}{\partial t}+\dfrac{\partial hU}{\partial x}=0,\\ \dfrac{\partial hU}{\partial t}+\dfrac{\partial}{\partial x}\left(hU^2+\beta h^3\psi+K\dfrac{gh^2}{2}\cos\theta\right)=g\cos\theta\left[h\left(\tan\theta-\mu_b\right)+\dfrac{10\lambda}{A^2B}\left(\psi-\dfrac{U^2}{4h^2}\right)\right],\\ \dfrac{\partial h\psi}{\partial t}+\dfrac{\partial hU\psi}{\partial x}=\dfrac{2gU\cos\theta}{h^2}\left[\dfrac{\alpha_1}{h^{1/2}}\left(U-\dfrac{2}{5}Ah^{3/2}\right)+\alpha_2\left(\psi-\dfrac{U^2}{4h^2}\right)\right],\end{cases}$$

where the expressions of A, B, C, α_1 and α_2 are

(5.2)
$$A=I_m\frac{\tan\theta-\mu_1}{\mu_2-\tan\theta}\frac{\sqrt{\phi g\cos\theta}}{d},\quad B=\frac{\mu_2-\mu_1}{(\mu_2-\tan\theta)(\tan\theta-\mu_1)},\quad C=\tan\theta\left(2\tan\theta-\frac{1}{B}\right),$$

$$\alpha_1=-\frac{33C}{2AB(34C+28)}\,,\qquad \alpha_2=\frac{77(9C-12)}{2A^2B(34C+28)}. \tag{5.3}$$

The parameters λ, β and K are given by

$$\lambda=\frac{847(4-3C)}{20(157C+84)},\quad \beta=\frac{11}{16}+\frac{5\lambda}{44},\quad K=1-\frac{3C}{4}+\frac{\lambda C}{7}, \tag{5.4}$$

and the basal friction μ_b is given by

$$\mu_b=\mu_1+\frac{\mu_2-\mu_1}{I_m\dfrac{2h^{3/2}\sqrt{\phi g\cos\theta}}{5dU}+1}. \tag{5.5}$$

The three characteristic velocities are

$$\lambda_0=U,\qquad \lambda_\pm=U\pm\sqrt{Kgh\cos\theta+3\beta h^2\psi}. \tag{5.6}$$

The system of equations (5.1) is hyperbolic if $K > 0$. It is in conservative form, with relaxation source terms. For the final expression (4.26) of λ or for $\lambda = 0$, the condition $K > 0$ is equivalent to the condition $C < 4/3$, which is also a condition for a well-posed system (see above in §4.3) and which is discussed in §6. If $K < 0$, the hyperbolicity is not guaranteed, which is not admissible.

The system admits the additional energy balance equation

$$\frac{\partial he}{\partial t} + \frac{\partial}{\partial x}\left(hUe + \Pi U\right) = gU\cos\theta\left[h(\tan\theta - \mu_b) + \frac{\beta\alpha_1}{h^{1/2}}\left(U - \frac{2}{5}Ah^{3/2}\right) + \left(\beta\alpha_2 + \frac{10\lambda}{A^2B}\right)\left(\psi - \frac{U^2}{4h^2}\right)\right] \tag{5.7}$$

where the specific energy is

$$e = \frac{U^2}{2} + \frac{\beta h^2\psi}{2} + K\frac{gh}{2}\cos\theta \tag{5.8}$$

and

$$\Pi = \beta h^3\psi + K\frac{gh^2}{2}\cos\theta. \tag{5.9}$$

The discontinuities that propagate at speed λ_0 are called contact discontinuities, while the two other are shocks (discontinuities). Across a shock, the quantities $m = h(U - \lambda_\pm)$ (conservation of mass) and ψ (conservation of enstrophy) are continuous. Furthermore, the jump of height h is constrained by the shock relation

$$m^2\left[\frac{1}{h}\right] + \beta\psi\left[h^3\right] + \frac{Kg\cos\theta}{2}\left[h^2\right] = 0, \tag{5.10}$$

where the notation $[f]$ stands for the jump of the quantity f.

It is important to note that the third equation of the system is the enstrophy equation and not the energy equation. This implies that, through a discontinuity, the enstrophy is conserved and the energy is dissipated. In the framework of hyperbolic systems of conservation laws, the energy is the mathematical entropy of the system.

5.2. **Reconstruction of the velocity field.** Since the model is derived consistently from the asymptotic expansions of the flow variables, it is possible to reconstruct the 2D-fields and, in particular, the variations of the velocity in the depth, from the values of the depth-averaged quantities calculated with the 1D-depth-averaged model. These velocity profiles are calculated at the same accuracy as the model. In the following, we show how to reconstruct in a consistent way the horizontal velocity field from the solution of (5.1), i.e. from the triplet (h, U, ψ).

Reverting to the dimensionless quantities, the expressions of $\tilde{u}^{(0)}$ at equilibrium (3.13) and of the averaged velocity $\tilde{U}^{(0)}$ (4.3) lead to

$$\tilde{u}^{(0)} = f(z)\tilde{U}^{(0)}, \tag{5.11}$$

where

$$f(z) = \frac{5}{3}\left[1 - \left(1 - \frac{z}{h}\right)^{3/2}\right] \tag{5.12}$$

is the renormalised Bagnold profile. From this relation, we deduce that an approximation of $\tilde{u}$ at order 0 is given by $\tilde{u} = f(z)\tilde{U} + O(\varepsilon)$. In order to have an

approximation of order 1, we expand

$$\tilde{u} = f(z)\tilde{U} + \varepsilon\left(\tilde{u}^{(1)} - f(z)\tilde{U}^{(1)}\right) + O(\varepsilon^2). \tag{5.13}$$

Thus we can obtain a consistent expression for $\tilde{u}$ by expressing consistently $\tilde{u}^{(1)} - f(z)\tilde{U}^{(1)}$ as a function of $(\tilde{h}, \tilde{U}, \tilde{\psi})$. After using (3.35) and (4.7) and some computations, we obtain

$$\tilde{u}^{(1)} - f(z)\tilde{U}^{(1)} = \tilde{A}B\frac{\partial \tilde{h}}{\partial \tilde{x}}\left[\frac{F^2\tilde{A}^2}{25\cos\theta}\tilde{h}^{7/2}f(z)\left(\frac{2}{5}f(z) - \frac{1}{2}\right) + C\tilde{h}^{3/2}\left(\frac{\tilde{z}}{\tilde{h}} - \frac{1}{2}f(z)\right)\right], \tag{5.14}$$

which yields, using (4.7) and (4.12),

$$\tilde{u}^{(1)} - f(z)\tilde{U}^{(1)} = f_1(z)\tilde{U}^{(1)} + f_2(z)\left(\tilde{\psi}^{(1)} - \frac{\tilde{A}\tilde{U}^{(1)}}{5\tilde{h}^{1/2}}\right), \tag{5.15}$$

where

$$f_1(z) = \frac{2C}{34C + 28}\left[2f(z)\left(\frac{11}{5}f(z) + 6\right) - 35\frac{z}{h}\right] \tag{5.16}$$

and

$$f_2(z) = \frac{55\tilde{h}^{1/2}}{A(17C/7 + 2)}\left[5C\left(\frac{z}{h} - \frac{1}{2}f(z)\right) - \frac{1}{5}(3C - 4)f(z)\left(\frac{2}{5}f(z) - \frac{1}{2}\right)\right]. \tag{5.17}$$

As we did before, we finally use (4.5) and (4.11) to replace the terms of first order in the right-hand side of (5.15) and, together with (5.13), we obtain, reverting to the dimensional quantities,

$$u = f(z)U + f_1(z)\left(U - \frac{2A}{5}h^{3/2}\right) + f_2(z)\left(\psi - \frac{U^2}{4h^2}\right). \tag{5.18}$$

This expression gives the velocity profile in the flow to the accuracy of the model, i.e. to within terms of order 2.

5.3. **Linear stability.** We study here the linear stability of a steady uniform solution of (5.1). In other words, we suppose that the solutions are sinusoidal perturbations of the constant solution given by $\tilde{h} = 1$, $\tilde{U} = \tilde{U}^{(0)}$ (see (4.3)) and $\tilde{\psi} = \tilde{\psi}^{(0)}$. The depth-averaged velocity can be scaled with its value in the constant solution, which yields $\tilde{A} = 5/2$, $\tilde{U}^{(0)} = 1$ and $\tilde{\psi}^{(0)} = 1/4$. We thus write $\tilde{h} = 1 + h'$, $\tilde{U} = 1 + U'$, $\tilde{\psi} = 1/4 + \psi'$, where $(h', U', \psi') = (a_1, a_2, a_3)\exp[ik(\tilde{x} - c\tilde{t})]$. The amplitudes a_1, a_2, a_3 are three constants, as well as the wave number k and the phase velocity c. We obtain the following linearised system:

$$M(\varepsilon)\,(h', U', \psi')^{\mathrm{T}} = 0, \qquad \text{with} \qquad M(\varepsilon) = \frac{\cos\theta}{F^2}R + i\varepsilon kL \tag{5.19}$$

where the matrix L comes from the conservative terms of the left-hand side of the equations, and is given by

$$L = \begin{pmatrix} 1 - c & 1 & 0 \\ \frac{3\beta}{4} + \frac{K\cos\theta}{F^2} & 1 - c & \beta \\ 0 & 0 & 1 - c \end{pmatrix}, \tag{5.20}$$

and the matrix R comes from the right-hand side relaxation terms and is given by

$$R = \begin{pmatrix} 0 & 0 & 0 \\ -\frac{3}{2B} - \frac{4\lambda}{5B} & \frac{1}{B} + \frac{4\lambda}{5B} & -\frac{8\lambda}{5B} \\ 3\tilde{\alpha}_1 - \tilde{\alpha}_2 & -2\tilde{\alpha}_1 + \tilde{\alpha}_2 & -2\tilde{\alpha}_2 \end{pmatrix}. \tag{5.21}$$

The dispersion relation is then obtained by imposing the condition $\det(M(\varepsilon)) = 0$. In order to obtain an analytical stability threshold in the limit $\varepsilon k \ll 1$, we expand $c = c^{(0)} + \varepsilon c^{(1)} + O(\varepsilon^2)$, which leads to $L = L^{(0)} + \varepsilon L^{(1)} + O(\varepsilon^2)$. We then obtain a similar expansion for the determinant of $M(\varepsilon)$, that we will denote $\det(M(\varepsilon)) = \delta^{(0)} + \varepsilon\delta^{(1)} + \varepsilon^2\delta^{(2)} + O(\varepsilon^3)$. We compute for the order 0 that $\delta^{(0)} = \det(\cos\theta R/F^2) = 0$. For the first order in ε, we find, after calculations,

$$\delta^{(1)} = ik\frac{2\cos^2\theta}{BF^4}\left(c^{(0)} - \frac{5}{2}\right)\left(\tilde{\alpha}_2 + \frac{8\lambda}{5}\tilde{\alpha}_1\right). \tag{5.22}$$

Hence the condition $\delta^{(1)} = 0$ yields $c^{(0)} = 5/2$. The matrix $L^{(0)}$ can thus be rewritten

$$L^{(0)} = \begin{pmatrix} -\frac{3}{2} & 1 & 0 \\ \frac{3\beta}{4} + \frac{K\cos\theta}{F^2} & -\frac{3}{2} & \beta \\ 0 & 0 & -\frac{3}{2} \end{pmatrix}. \tag{5.23}$$

For the order 2 in ε, we obtain

$$\delta^{(2)} = \left[\frac{2ik\cos^2\theta}{BF^4}c^{(1)} - \frac{k^2\cos\theta}{2F^2}\left(-\frac{25}{4} + \frac{(4-3C)\cos\theta}{F^2}\right)\right]\left(\tilde{\alpha}_2 + \frac{8\lambda\tilde{\alpha}_1}{5}\right). \tag{5.24}$$

Solving $\delta^{(2)} = 0$ then yields

$$c^{(1)} = i\frac{kB}{4\cos\theta}\left(\frac{25}{4}F^2 - (4-3C)\cos\theta\right). \tag{5.25}$$

The condition of stability is $\mathrm{Im}(c^{(1)}) < 0$, which gives $25F^2/4 < (4-3C)\cos\theta$. A consistent expression of the stability criterion for the $\mu(I)$ rheology was obtained by Forterre (2006), using a slightly different Froude number $\mathcal{F}$, defined as $\mathcal{F}^2 = F^2/\cos\theta$. With this definition of the Froude number, the obtained stability criterion is exactly the same as found by Forterre (2006) and it reads

$$\mathcal{F} < \mathcal{F}_c = \frac{4}{5}\sqrt{1 - \frac{3C}{4}} = \frac{4}{5}\sqrt{1 - \frac{3}{2}\tan^2\theta + \frac{3}{4}\frac{(\mu_2 - \tan\theta)(\tan\theta - \mu_1)}{\mu_2 - \mu_1}\tan\theta}. \tag{5.26}$$

The stability criteria are identical because the present depth-averaged model is consistent up to order 1 in ε with the $\mu(I)$ rheology.

Note that the critical Froude number $\mathcal{F}_c$ is real if the condition $C < 4/3$ is satisfied. This condition is also a condition for a well-posed enstrophy equation (see §4.3 above) and to guarantee the hyperbolicity of the system (see §5.1). Since this condition appears in the stability criterion of a steady uniform flow for the $\mu(I)$ rheology, it is not specific to the model derived in this work. This condition is discussed in §6.

The variation of the consistent critical Froude number (present model and Forterre (2006)) as a function of the inclination is presented in Figure 2 (red curve) in the case of glass beads, using the values $\mu_1 = \tan 20.9°$ and $\mu_2 = \tan 32.76°$ (Jop et al., 2005), together with the experimental measurements of Forterre and Pouliquen (2003) (black dots). The stability criterion obtained with a Saint-Venant model

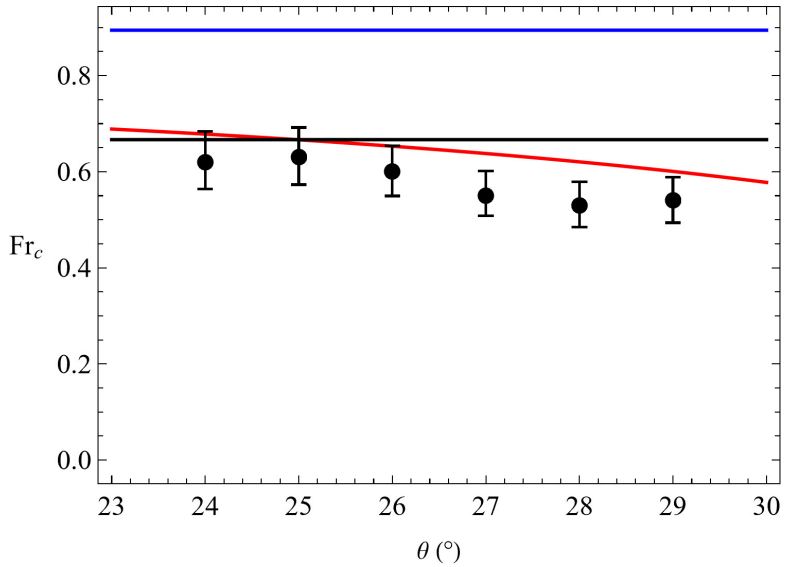

FIGURE 2. Critical Froude number as a function of the angle θ for glass beads. Theoretical value obtained with the $\mu(I)$ rheology (Forterre, 2006) and given by the present model (red curve). Saint-Venant model with a shape factor of 1 (black line) and of 5/4 (blue line) (Forterre and Pouliquen, 2003). Black dots: experimental measurements of Forterre and Pouliquen (2003).

(Forterre and Pouliquen, 2003) is also shown, with a shape factor of 1 (velocity constant over the depth) (black line), or with a shape factor of 5/4 (Bagnold velocity profile) (blue line). These criteria differ from the criterion obtained with the $\mu(I)$ rheology because these Saint-Venant models, both with a shape factor of 1 or 5/4, are inconsistent approximations of the governing equations. The criterion obtained with a constant velocity profile ($\mathcal{F}_c = 2/3$) is closer to the consistent criterion but the velocity profile of the steady uniform flows is not a Bagnold profile. With a shape factor of 5/4, the velocity profile is a Bagnold profile but the value of the critical Froude number ($\mathcal{F}_c = 0.89$) is far from the consistent value, because important terms were neglected in the derivation of the model. The systematic asymptotic expansions used to derive the present model enables to obtain both a consistent stability criterion and a Bagnold velocity profile for steady uniform flows with its correction for flows in a non-equilibrium state.

Using the dispersion relation, it is also possible to express $k = k(\omega, F)$, where $\omega = ck$. It is then possible to study the neutral stability curve defined by $\mathrm{Im}(\omega) = 0$. Computations (not shown here) show that $\partial F_c/\partial\omega|_{\omega=0} = 0$ and that $\partial^2 F_c/\partial\omega^2|_{\omega=0} = f(\lambda)$, where λ is the parameter introduced in Section 4.2 and $f(\lambda)$ is a complicated function of λ which vanishes when λ has the value (4.26). For this value of λ, the neutral stability curve $F = F(\omega)$ is obtained at a fixed value of the Froude number independently of the frequency ω. This behaviour is typical of first-order models in other rheologies. For this reason and for reasons discussed below, this particular value of λ is the final choice for the model.

5.4. **Adding diffusive effects.** First-order models such as the present model (5.1) lead to some discrepancies due to the absence of diffusive terms (Forterre, 2006; Andreotti et al., 2013; Gray and Edwards, 2014). The spatial growth rate in particular is not accurate far from the long-wave limit and the stabilisation of high frequencies is not predicted. Therefore it is important to add diffusive terms to the model. These effects are of second order with respect to ε but, since the second-order full consistency is very complicated and, moreover, does not yield well-posed models, only the linear terms due to the stress gradient in the stream-wise direction are considered. The integration of (2.31) can be written

(5.27)
$$\frac{\partial \tilde{h}\tilde{U}}{\partial \tilde{t}}+\frac{\partial}{\partial \tilde{x}}\left(\tilde{h}\tilde{U}^2+\tilde{h}^3\tilde{\psi}\right)=\frac{1}{\varepsilon\phi F^2}\left(\phi\sin\theta\tilde{h}-\varepsilon\frac{\partial}{\partial\tilde{x}}\int_0^{\tilde{h}}\tilde{p}\mathrm{d}\tilde{z}-\tilde{\tau}_{xz}(0)+\varepsilon^2\int_0^{\tilde{h}}\frac{\partial\tilde{\tau}_{xx}}{\partial\tilde{x}}\mathrm{d}\tilde{z}\right).$$

In this equation, only the second-order terms given by the integral of $\partial\tilde{\tau}_{xx}/\partial\tilde{x}$ are kept.

Equation (3.17) yields

(5.28)
$$\frac{\partial\tilde{\tau}_{xx}^{(0)}}{\partial\tilde{x}}=\phi\sin\theta\left\{\left(\frac{\partial\tilde{h}}{\partial\tilde{x}}\right)^2\left[\left(1-\frac{\tilde{z}}{\tilde{h}}\right)^{1/2}+\left(1-\frac{\tilde{z}}{\tilde{h}}\right)^{-1/2}-2\right]+2\frac{\partial^2\tilde{h}}{\partial\tilde{x}^2}\left[\tilde{h}^{1/2}(\tilde{h}-\tilde{z})^{1/2}-\tilde{h}+\tilde{z}\right]\right\},$$

which leads to

$$\int_0^{\tilde{h}}\frac{\partial\tilde{\tau}_{xx}^{(0)}}{\partial\tilde{x}}\,\mathrm{d}\tilde{z}=\frac{1}{3}\phi\sin\theta\frac{\partial}{\partial\tilde{x}}\left(\tilde{h}^2\frac{\partial\tilde{h}}{\partial\tilde{x}}\right). \tag{5.29}$$

Using the expression (4.3) of $\tilde{U}^{(0)}$, this term can be written as a diffusive term

$$\int_0^{\tilde{h}}\frac{\partial\tilde{\tau}_{xx}^{(0)}}{\partial\tilde{x}}\,\mathrm{d}\tilde{z}=\phi F^2\frac{\partial}{\partial\tilde{x}}\left(\tilde{\nu}_{\text{eff}}\tilde{h}\frac{\partial\tilde{U}^{(0)}}{\partial\tilde{x}}\right), \tag{5.30}$$

with an effective viscosity

$$\tilde{\nu}_{\text{eff}}=\frac{5\sin\theta}{9\tilde{A}F^2}\tilde{h}^{1/2}. \tag{5.31}$$

Defining $\tilde{\alpha}_\nu$ by $\tilde{\nu}_{\text{eff}}=\tilde{\alpha}_\nu\tilde{h}^{1/2}$, we can write the depth-averaged momentum balance equation

(5.32)
$$\frac{\partial\tilde{h}\tilde{U}}{\partial\tilde{t}}+\frac{\partial}{\partial\tilde{x}}\left(\tilde{h}\tilde{U}^2+\beta\tilde{h}^3\tilde{\psi}+K\frac{\cos\theta\tilde{h}^2}{2F^2}\right)=\frac{\cos\theta}{\varepsilon F^2}\left[\tilde{h}(\tan\theta-\mu_b)+\frac{10\lambda}{\tilde{A}^2B}\left(\tilde{\psi}-\frac{\tilde{U}^2}{4\tilde{h}^2}\right)\right]$$

$$+\varepsilon\frac{\partial}{\partial\tilde{x}}\left(\tilde{\alpha}_\nu\tilde{h}^{3/2}\frac{\partial\tilde{U}}{\partial\tilde{x}}\right). \tag{5.33}$$

The dimensionless effective viscosity obtained in Gray and Edwards (2014) is similar, apart from a coefficient $1/F^2$ which comes from a different scaling. The expression of the effective viscosity in Forterre (2006) is different but it is consistent at order 0 with (5.31).

We now need to take the diffusion into account in the energy equation. Technical details are given in Appendix B. Since we consider only linear terms, there is some freedom of choice for non-linear terms that inevitably appear either in the enstrophy

equation or in the energy equation or both. As for the first-order hyperbolic model, we impose conservation of enstrophy and dissipation of energy. Therefore, the enstrophy equation is written without non-linear terms, which implies dissipative non-linear terms in the energy equation. The enstrophy balance equation is thus written

(5.34)
$$\frac{\partial \tilde{h}\tilde{\psi}}{\partial \tilde{t}}+\frac{\partial \tilde{h}\tilde{U}\tilde{\psi}}{\partial \tilde{x}}=\frac{2\tilde{U}\cos\theta}{\varepsilon\tilde{h}^2F^2}\left[\frac{\tilde{\alpha}_1}{\tilde{h}^{1/2}}\left(\tilde{U}-\frac{2}{5}\tilde{A}\tilde{h}^{3/2}\right)+\tilde{\alpha}_2\left(\tilde{\psi}-\frac{\tilde{U}^2}{4\tilde{h}^2}\right)\right]+\varepsilon\frac{\partial}{\partial\tilde{x}}\left(\frac{16\tilde{\alpha}_\nu}{7\beta}\tilde{h}^{3/2}\frac{\partial\tilde{\psi}}{\partial\tilde{x}}\right).$$

The new depth-averaged energy balance equation is now found from the three equations of the system and can be written

$$\begin{aligned}(5.35)\quad &\frac{\partial}{\partial\tilde{t}}\left(\tilde{h}\frac{\tilde{U}^2}{2}+\frac{\beta\tilde{h}^3\tilde{\psi}}{2}+K\frac{\tilde{h}^2\cos\theta}{2F^2}\right)+\frac{\partial}{\partial\tilde{x}}\left(\frac{\tilde{h}\tilde{U}^3}{2}+\frac{3\beta\tilde{h}^3\tilde{U}\tilde{\psi}}{2}+K\frac{\tilde{h}^2\tilde{U}\cos\theta}{F^2}\right)\\ &=\frac{\tilde{U}\cos\theta}{\varepsilon F^2}\left[\tilde{h}(\tan\theta-\mu_b)+\frac{\beta\tilde{\alpha}_1}{\tilde{h}^{1/2}}\left(\tilde{U}-\frac{2}{5}\tilde{A}\tilde{h}^{3/2}\right)+\left(\beta\tilde{\alpha}_2+\frac{10\lambda}{\tilde{A}^2B}\right)\left(\tilde{\psi}-\frac{\tilde{U}^2}{4\tilde{h}^2}\right)\right]\\ &+\varepsilon\frac{\partial}{\partial\tilde{x}}\left(\tilde{\alpha}_\nu\tilde{h}^{3/2}\tilde{U}\frac{\partial\tilde{U}}{\partial\tilde{x}}\right)+\varepsilon\frac{\partial}{\partial\tilde{x}}\left(\frac{8\tilde{\alpha}_\nu}{7\beta}\tilde{h}^{7/2}\frac{\partial\tilde{\psi}}{\partial\tilde{x}}\right)-\varepsilon\tilde{\alpha}_\nu\tilde{h}^{3/2}\left(\frac{\partial\tilde{U}}{\partial\tilde{x}}\right)^2-\varepsilon\frac{16\tilde{\alpha}_\nu}{7\beta}\tilde{h}^{5/2}\frac{\partial\tilde{h}}{\partial\tilde{x}}\frac{\partial\tilde{\psi}}{\partial\tilde{x}}.\end{aligned}$$

Reverting to the dimensional quantities, the system can be written

$$(5.36)\qquad \frac{\partial h}{\partial t}+\frac{\partial hU}{\partial x}=0,$$

(5.37)
$$\frac{\partial hU}{\partial t}+\frac{\partial}{\partial x}\left(hU^2+\Pi\right)=g\cos\theta\left[h\left(\tan\theta-\mu_b\right)+\frac{10\lambda}{A^2B}\left(\psi-\frac{U^2}{4h^2}\right)\right]+\frac{\partial}{\partial x}\left(\alpha_\nu h^{3/2}\frac{\partial U}{\partial x}\right),$$

(5.38)
$$\frac{\partial h\psi}{\partial t}+\frac{\partial hU\psi}{\partial x}=\frac{2gU\cos\theta}{h^2}\left[\frac{\alpha_1}{h^{1/2}}\left(U-\frac{2}{5}Ah^{3/2}\right)+\alpha_2\left(\psi-\frac{U^2}{4h^2}\right)\right]+\frac{\partial}{\partial x}\left(\frac{16\alpha_\nu}{7\beta}h^{3/2}\frac{\partial\psi}{\partial x}\right),$$

with the expressions of A and B given in (5.2), of α_1 and α_2 in (5.3), of λ and K in (5.4), of the basal friction μ_b in (5.5), with

$$(5.39)\qquad \alpha_\nu=\frac{5g\sin\theta}{9A}$$

and with

$$(5.40)\qquad \Pi=\beta h^3\psi+K\frac{gh^2}{2}\cos\theta.$$

The system admits the energy balance equation

$$\begin{aligned}(5.41)\quad &\frac{\partial he}{\partial t}+\frac{\partial}{\partial x}\left(hUe+\Pi U\right)\\ &=gU\cos\theta\left[h(\tan\theta-\mu_b)+\frac{\beta\alpha_1}{h^{1/2}}\left(U-\frac{2}{5}Ah^{3/2}\right)+\left(\beta\alpha_2+\frac{10\lambda}{A^2B}\right)\left(\psi-\frac{U^2}{4h^2}\right)\right]\\ &+\frac{\partial}{\partial x}\left(\alpha_\nu h^{3/2}U\frac{\partial U}{\partial x}\right)+\frac{\partial}{\partial x}\left(\frac{8\alpha_\nu}{7\beta}h^{7/2}\frac{\partial\psi}{\partial x}\right)-\alpha_\nu h^{3/2}\left(\frac{\partial U}{\partial x}\right)^2-\frac{16\alpha_\nu}{7\beta}h^{5/2}\frac{\partial h}{\partial x}\frac{\partial\psi}{\partial x}\end{aligned}$$

with the specific energy e given by (5.8).

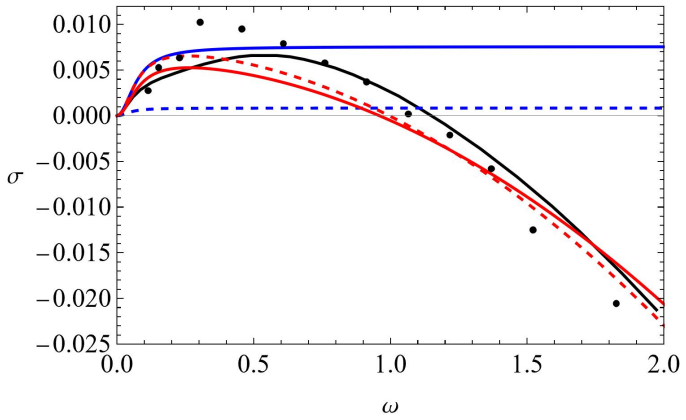

FIGURE 3. Spatial dimensionless growth rate for $\theta = 29°$ and $\mathcal{F} = 1.02$ as a function of the dimensionless frequency. Black dots: experimental measures of Forterre and Pouliquen (2003). Red solid curve: present model with diffusion. Black curve : theoretical result for the $\mu(I)$ rheology (Forterre, 2006). Saint-Venant model (Forterre and Pouliquen, 2003) with a shape factor of 1 (blue solid curve) and 5/4 (blue dashed curve). Red dashed curve: model of Gray and Edwards (2014).

The dispersion relation is modified by the diffusive terms. Taking again sinusoidal perturbations of the form $\tilde{h} = 1+h'$, $\tilde{U} = \tilde{U}^{(0)}+U'$ and $\tilde{\psi} = \tilde{\psi}^{(0)}+\psi'$, the linearized system now reads

$$M_V(\varepsilon)\begin{pmatrix} h' \\ U' \\ \psi' \end{pmatrix} = 0, \qquad \text{with} \qquad M_V(\varepsilon) = \frac{\cos\theta}{F^2}R + i\varepsilon k L + \varepsilon^2 k^2 \tilde{\alpha}_\nu V, \tag{5.42}$$

where R, L are defined in (5.21), (5.20) and V is the matrix of the linearized viscous terms, given by

$$V = \begin{pmatrix} 0 & 0 & 0 \\ 0 & 1 & 0 \\ 0 & 0 & \frac{16}{7\beta} \end{pmatrix}. \tag{5.43}$$

The new dispersion relation is $\det(M_V) = 0$. We now suppose that $\omega = ck \in \mathbb{R}$ and that k is complex. The spatial growth rate is then given by $\sigma = -\mathrm{Im}(k)$. The system is stable if and only if $\sigma < 0$.

The variations of the dimensionless spatial growth rate σ with the dimensionless angular frequency is presented in Figure 3 for the present model with diffusion (red solid curve) in the case of glass beads ($\mu_1 = \tan 20.9°$, $\mu_2 = \tan 32.76°$, Jop et al. (2005)) and for $\theta = 29°$ and $\mathcal{F} = 1.02$. The results are compared with the theoretical results obtained for the $\mu(I)$ rheology by Forterre (2006) (black curve) and with the experimental measures of Forterre (2006) (black dots). The Saint-Venant models derived with a constant velocity profile (blue solid curve) and with a Bagnold profile (blue dashed curve) are also presented together with the model of (Gray and Edwards, 2014) with diffusion (red dashed curve).

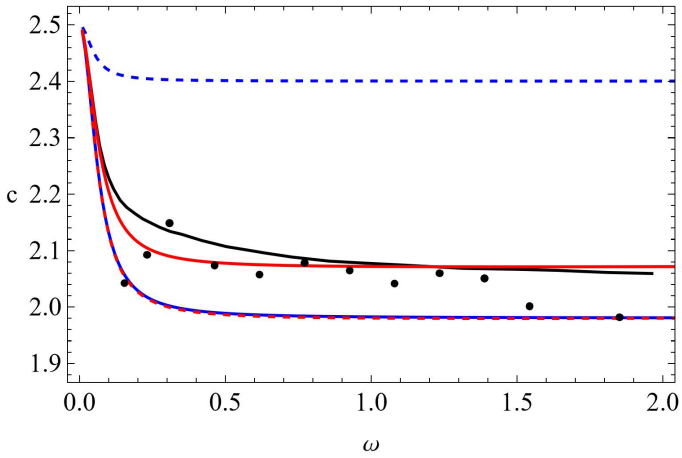

FIGURE 4. Dimensionless phase velocity for $\theta = 29°$ and $\mathcal{F} = 1.02$ as a function of the dimensionless frequency. Black dots: experimental measures of Forterre and Pouliquen (2003). Red solid curve: present model with diffusion. Black curve : theoretical result for the $\mu(I)$ rheology (Forterre, 2006). Saint-Venant model (Forterre and Pouliquen, 2003) with a shape factor of 1 (blue solid curve) and 5/4 (blue dashed curve). Red dashed curve: model of Gray and Edwards (2014).

The curve obtained with the present model with diffusion is very close to the curve obtained by (Gray and Edwards, 2014). Both models predict quite correctly the stabilization of high frequencies, with a cutoff frequency, and are in reasonable agreement with the experimental measures and with the theoretical result for the $\mu(I)$ rheology. By contrast, the Saint-Venant models cannot predict the cutoff frequency due to the absence of diffusive terms. These Saint-Venant models are also inconsistent approximations of the governing equations but the inaccuracy is much more important for the model with a shape factor of 5/4 (Bagnold profile). The present model is also based on a Bagnold velocity profile at leading order but it gives accurate results because of the consistent asymptotic expansions used in its derivation.

The dimensionless phase velocity c is presented in Figure 4 (same conditions as for Figure 3). The present model with diffusion (red curve) is in good agreement with the theoretical result for the $\mu(I)$ rheology (black curve) and with the experimental measures (Forterre, 2006). The model of Gray and Edwards (2014) (red dashed curve) gives practically the same result as the Saint-Venant model with a flat velocity profile (blue solid curve) (Forterre and Pouliquen, 2003), while the Saint-Venant model with a Bagnold profile ($\alpha = 5/4$) gives values clearly too large. In this case again, the consistent derivation used for the present model improves the accuracy of the predictions when a Bagnold velocity profile is considered for steady uniform flows.

The variations of the dimensionless cutoff angular frequency ω_c as a function of the Froude number above criticality $\mathcal{F} - \mathcal{F}_c$ is presented in Figure 5 for glass beads and $\theta = 29°$. The effect of the parameter λ is shown with the model with diffusion

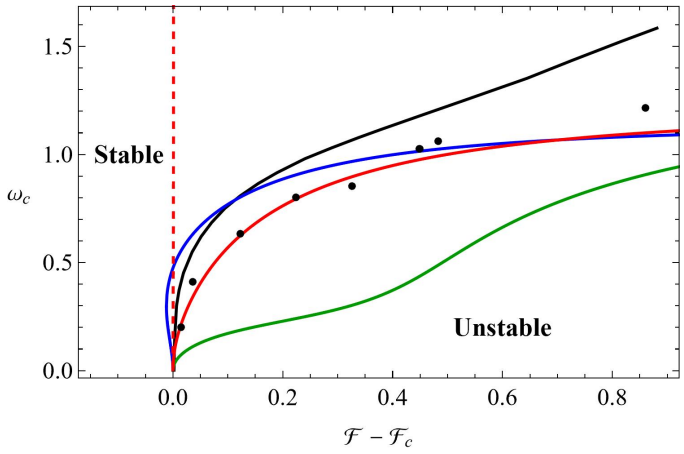

FIGURE 5. Dimensionless cutoff frequency ω_c of the instability as a function of the Froude number above criticality $\mathcal{F} - \mathcal{F}_c$ for $\theta = 29°$. Black dots: experimental measures of Forterre and Pouliquen (2003). Present model with diffusion for λ given by (4.26) (red solid curve), $\lambda = 0$ (blue curve) and $\lambda = 11/4$ (green curve). Red dashed curve: present model without diffusion for λ given by (4.26). Black curve: theoretical result for the $\mu(I)$ rheology (Forterre, 2006).

in three cases: λ is equal to the critical value (4.26) (red solid curve), $\lambda = 0$ (blue curve) and $\lambda = 11/4$ (green curve). In the case $\lambda = 0$, there is no relaxation term for the enstrophy in the momentum balance equation and the first-order correction to the granular friction law is entirely written as terms in the momentum flux. In the case $\lambda = 11/4$, we have $\beta = 1$, which means that there is no correction on the shear term $h^3\psi$ in the momentum flux although, since $K < 1$, there is still a correction on the pressure term of the momentum flux (the value of λ needed to have $K = 1$ is $21/4$, so even higher). In the final choice (4.26), part of the first-order correction is written in the momentum flux, with a correction on both the enstrophy and pressure terms, and another part as a relaxation term. This critical value of λ is chosen to have a cutoff frequency independent of the Froude number for the model without diffusion (red dashed line). All values of λ give the same result in the validity domain of the shallow-water approximation, thus for small frequencies, but this domain is quite small ($\tilde{\omega} < 0.1$ approximately). For larger frequencies, the cutoff frequency is quite sensitive to the choice of λ. For the critical value of λ (4.26), the agreement of the model with diffusion with the theoretical result for the $\mu(I)$ rheology (black curve) and with the experimental results (black dots), both obtained by Forterre (2006), is quite good. For smaller values of λ, and in particular for $\lambda = 0$, there are unstable frequencies that are smaller than the cutoff at the long-wave limit, which does not seem to be observed experimentally. For larger values of λ, the cutoff frequency is too small. The diffusion is again important to stabilize the high frequencies. Only the case $\theta = 29°$ is presented, but other values of θ studied by Forterre (2006) and Gray and Edwards (2014) show the same trends.

5.5. **Numerical resolution.** In this subsection, we solve numerically the model in order to study the roll waves instability. The numerical solution is calculated

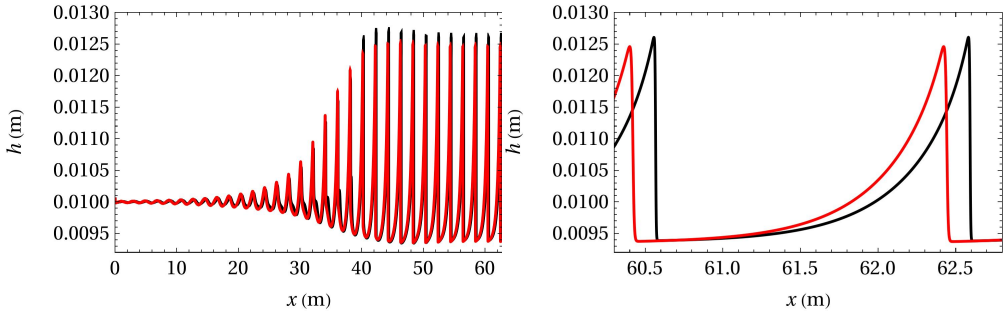

FIGURE 6. Profile of height for the roll-wave instability. In black: System (5.1) (purely hyberbolic). In red: System (5.36)–(5.38) (system with diffusion).

with a Godunov type scheme (HLLC Riemann solver). We solve system (5.1) in the variables (h, U, ψ). In these variables, the total energy plays the role of a mathematical entropy for the system. The relaxation source terms are implemented explicitly. The second-order diffusion terms are approximated by centered finite differences. We use the following parameters: $\mu_1 = \tan(20.9°)$, $\mu_2 = \tan(32.76°)$, $I_m = 0.279$ (see Jop et al. (2006)), $d = 5 \times 10^{-4}$ m, $\theta = 25°$, $\phi = 0.6 - 0.2\, I^{(0)}$ (see (3.10)), $g = 9.81$ m/s, and $h_0 = 10^{-2}$ m. It follows that $\mathcal{F} \approx 0.806 > \mathcal{F}_c \approx 0.666$.

We initialize the system with a steady solution, that we perturb at the left of the domain by imposing a sinusoidal boundary condition of small relative amplitude for the function h. In the beginning, the amplitude of the perturbation increases exponentially. After some time, the amplitude converges to a maximal value. A stationary state is then reached and the solution becomes periodic. This is illustrated by Figure 6 which shows the height of the flow, for the system (5.1) (purely hyperbolic) and for the system (5.36)–(5.38) (with diffusion terms). The depth profiles of the two system are similar. It can be seen that, in presence of diffusion, the amplitude of the waves is slightly smaller and the propagation is slightly slowed. As expected, the shock is steeper in the purely hyperbolic model. However, the effects of the diffusive terms seem to have little overall impact on the global shape of the solution. This is coherent with the fact that the diffusive terms are of order ε^2 in our asymptotic. Figure 7 shows the values taken by the basal friction μ_b and the enstrophy ψ over a period, once the stationary state is reached. The basal friction decreases when the depth increases, while the enstrophy increases.

Finally, the horizontal velocity profile is reconstructed in Figure 8, with the help of Equation (5.18). The reconstructions are presented for three different values of x. The black curve is obtained by reconstruction of the velocity at the wave trough. It is very close to a Bagnold profile (solution at equilibrium). The red curve is obtained by reconstruction at the wave crest. The blue curve is obtained at an intermediary state. As the height increases, the profile becomes more and more curved. The first-order correction with respect to the leading-order velocity profile, which represents the deviation of the velocity profile from the Bagnold profile, can be visualized by the difference between a curve (red or blue) and the black curve.

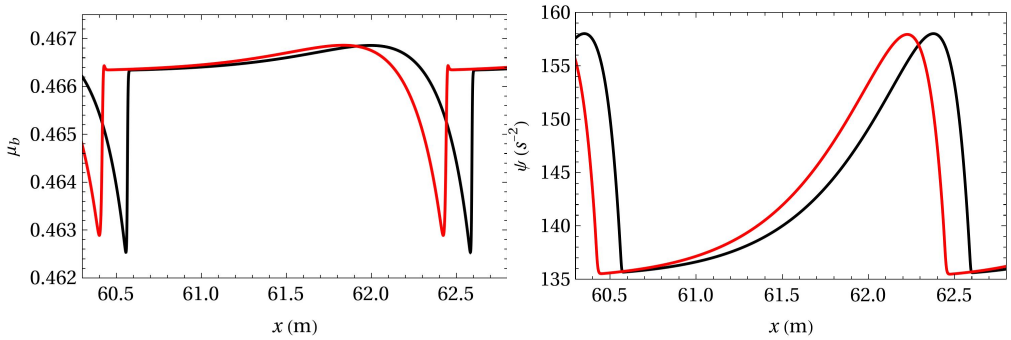

FIGURE 7. Profile of μ_b and of ψ for the roll-wave instability. In black: System (5.1) (purely hyberbolic). In red: System (5.36)–(5.38) (system with diffusion).

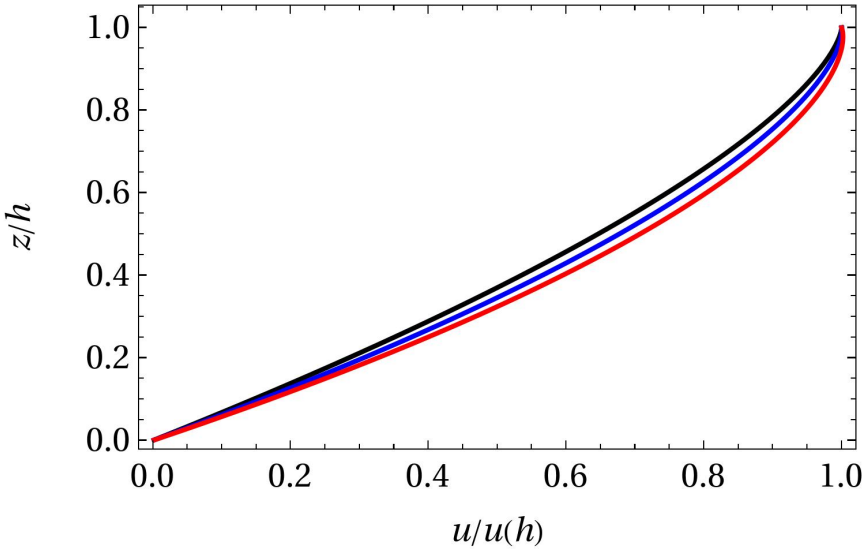

FIGURE 8. Reconstruction of the velocity profile for the numerical simulation of Section 5.5. In black, profile at the minimal value of the perturbation of the height (just after the shock). In red, profile at the maximal value of the perturbation. In blue, profile where the height of the perturbation reaches eighty percent of the maximal height.

6. Need for model regularization

It is essential to regularize the model for certain values of the angle θ because some quantities of the system (5.36)–(5.38) may change sign or become infinite, resulting in a ill-posed model.

In order to understand why this can happen, let us recall some facts about the $\mu(I)$ rheology. As mentioned in the first section, this rheology corresponds to a

friction law, for which the friction coefficient is given by

$$\mu(I) = \mu_1 + \frac{\mu_2 - \mu_1}{1 + I_m/I}. \tag{6.1}$$

The two parameters μ_1 and μ_2 are determined experimentally. They characterize the angles for which steady uniform flows can be observed. These steady uniform flows only exist when

$$\mu_1 < \tan\theta < \mu_2. \tag{6.2}$$

Outside this range, there is no equilibrium and all the formulas that we obtained previously do not make any sense a priori. We insist on the fact that the model (5.36)–(5.38) is derived with an asymptotic method, under the hypotheses that θ is constant and inside this range, so that the flow remains close to the uniform stationary flow. However, for geophysical applications, the value of the slope may not lie within the interval $[\mu_1, \mu_2]$.

Recall that the expression of the inertial number I at leading order is

$$I^{(0)} = I_m \frac{\tan\theta - \mu_1}{\mu_2 - \tan\theta}. \tag{6.3}$$

This expression is only valid when the condition (6.2) is verified and makes no sense otherwise.

- In the limit $\tan\theta \to \mu_1$, we have $I^{(0)} \to 0$. It follows that $U^{(0)}$ and $\psi^{(0)}$ both converge to 0 and the flow should stop. This is called the liquid/solid transition. In the right-hand side of the system (5.36)–(5.38), the relaxation coefficients as well as the diffusion coefficients diverge to $+\infty$, which indicates that U and ψ should go to zero instantaneously. Given that this is likely to cause problems for numerical resolution and that the instantaneous stopping of an avalanche is not physical, these coefficients need to be regularized.
- In the limit $\tan\theta \to \mu_2$, $I^{(0)} \to +\infty$. The relaxation and diffusion coefficients go to zero. This is the liquid/gas transition, after which the flow becomes uniformly accelerated and enters a kinetic regime in which the volume fraction decreases. For $\tan\theta > \mu_2$, the effective viscosity becomes negative, requiring regularization.
- Finally, another singularity of the model can appear when the coefficient μ_2 is large. Indeed, recall that the stability criterion in the long wave limit is

$$\mathcal{F}^2 < \mathcal{F}_c^2 = \frac{16}{25}(4 - 3C), \tag{6.4}$$

  where $C = C(\theta)$ is an increasing function of θ which is equal to $2\mu_2^2$ when $\tan\theta = \mu_2$. If $\mu_2 < \sqrt{2/3}$, the condition $C < 4/3$ is automatically satisfied for a slope in the range $[\mu_1, \mu_2]$. If $\mu_2 > \sqrt{2/3} \approx 0.816$, there are some values of θ which verify (6.2) for which every steady flow is unstable, even when $\mathcal{F} = 0$, because $C > 4/3$ (which gives $\mathcal{F}_c^2 < 0$!). This phenomenon is inherent to the $\mu(I)$ rheology since the stability criterion is the same for the bulk equations, as shown by Forterre (2006). In the system (5.36)–(5.38), it is materialised by the fact that the sign of the relaxation coefficient α_2 changes when the critical Froude number is equal to zero (see §4.3 above), as well as the sign of the coefficient K in front of the hydrostatic pressure

and of the potential energy term in the expression (5.8) of the energy. In particular, the enstrophy ψ grows exponentially in this case and the system is ill-posed. Furthermore, the hyperbolicity of the system is not guaranteed anymore when $C > 4/3$ (see §5.1). It is not clear whether this instability effect has a real physical meaning or if it is only a default of the rheology. In the literature, the value of μ_2 is often lower than the critical value $\sqrt{2/3}$ ($\mu_2 = \tan 32.76^\circ \approx 0.643$ in the paper of Jop et al. (2006) for instance). However, the value of μ_2 was $\mu_2 = 1$ for the experiments of Börzsönyi and Ecke (2006). They observed steady flows only under a critical angle $\tan\theta \approx 0.85$, above which the flow becomes uniformly accelerated. With their parameters, this corresponds to a value of $C(\theta) \approx 1.36$, which is close to the theoretical value $C = 4/3 \approx 1.33$ that we obtain for the instability of the model. Further investigations need to be performed to see whether this is a coincidence or a successful prediction of the $\mu(I)$ rheology. In any case, this instability also requires regularization.

A regularized system should be usable for numerical simulations with any value of the slope. However, the development of such a regularized model requires an in-depth study of flow stopping, of accelerated flows and of granular avalanche fronts, which is beyond the scope of this article and will be the subject of a future work.

7. Conclusion

In this work, we derive a new depth-averaged model for an incompressible granular flow described by the $\mu(I)$ rheology. The derivation is made using a consistent asymptotic method under the assumption of shallow flows. This method implies that the model is consistent at the first order, with respect to the small shallow-flow parameter, with the $\mu(I)$ rheology. In particular, the first-order correction to the classical granular friction law is included in the model. The resulting three-equation model is a hyperbolic system of conservation laws for the flow depth, the depth-averaged velocity and an additional quantity, called enstrophy, which takes into account shear effects. This system admits an exact energy balance equation. For steady uniform flows, the model is consistent with a Bagnold velocity profile, which is found at leading order. Otherwise the model includes the first-order correction to this profile. The model is mathematically well-posed, with a classical structure well-suited for numerical resolution. Since the model is consistent, it gives the exact stability criterion of the $\mu(I)$ rheology in the long-wave limit as found by Forterre (2006).

Thanks to the consistency of the asymptotic method used for the derivation, the variation in the depth of the velocity can be reconstructed explicitly with the three variables of the depth-averaged model. The deviations to the Bagnold profile can thus be calculated for flows which are not steady and uniform, such as granular roll waves.

This hyperbolic model is also extended to include diffusive effects. The spatial growth rate and the phase velocity predicted by this extended model is in good agreement with both the theoretical predictions of the $\mu(I)$ rheology and with the experimental data of Forterre and Pouliquen (2003). In particular, the extended model predicts successfully the stabilization of high frequencies and the variation of the cutoff frequency with the Froude number. In this respect, it is important to note that it is possible to derive an infinite number of consistent models, all of which are

equivalent within the validity domain of the long-wave approximation, but differ outside this domain. The variation of the cutoff frequency with the Froude number was used to select the best variant among the different possible consistent models according to its extrapolation capabilities outside the shallow-flow domain.

Numerical simulations of granular roll waves are presented, using classical finite-volume schemes with an approximate Riemann solver. All depth-averaged quantities can be calculated and the velocity profiles in the depth can be easily reconstructed.

The asymptotic method used to derive the model assumes that the flow remains close to the steady uniform flow and therefore that such a steady uniform flow exists. In the context of the $\mu(I)$ rheology, a steady uniform flow is only possible within a certain range of the angle of inclination of the bottom with respect to the horizontal. This range defines the model's domain of validity. Outside this range, certain model quantities become infinite or change sign, and the model becomes mathematically ill-posed. This problem is related to the solid/liquid and liquid/gas transitions, which are well-known limits of the $\mu(I)$ rheology. A regularization of the model is therefore necessary for these transitions, based on the study of flow stopping, accelerated flows and avalanche fronts, and will be the subject of a future work.

The model has been derived under the assumption of incompressible flows, but dilatancy phenomena can be significant in practice. A further development of this work will be to take into account variations in volume fraction with the inertial number according to the phenomenological expressions of the local rheology proposed in the literature. A further development will concern granular flows on smooth bottoms, for which a non-zero slip velocity on the bottom is possible and can play an important role, in particular for granular jumps.

Acknowledgements. The authors thank Thierry Faug for helpful assistance and discussions.

Funding. This project was supported by the institute of Mathematics for Planet Earth (iMPT) and by the Department AQUA of INRAE.

Declaration of interests. The authors report no conflict of interest.

Appendix A. Derivation of the depth-averaged energy equation

We compute the right-hand-side of (4.30). In order to do this, we use the expansion (4.19) to keep track of the friction law (4.17). We first compute

$$\begin{aligned}\frac{\partial \tilde{\tau}_{xz}}{\partial \tilde{z}} =& \frac{\partial}{\partial \tilde{z}}\left(\tilde{\tau}_{xz}^{(0)} + \varepsilon \tilde{\tau}_{xz}^{(1)}\right) + O(\varepsilon^2) = -\mu^{(0)}\phi\cos\theta + \varepsilon\frac{\partial \tilde{\tau}_{xz}^{(1)}}{\partial \tilde{z}} + O(\varepsilon^2)\\ =& -\mu_b\phi\cos\theta + \varepsilon\phi\cos\theta\frac{\tilde{U}^{(1)}}{B\tilde{U}^{(0)}} + \varepsilon\frac{\partial \tilde{\tau}_{xz}^{(1)}}{\partial \tilde{z}} + O(\varepsilon^2),\end{aligned} \tag{A.1}$$

where the last equality comes from (4.19). We obtain with (3.13) and (3.24)

$$\begin{aligned}\int_0^{\tilde{h}} \tilde{u}\frac{\partial \tilde{\tau}_{xz}}{\partial \tilde{z}}\mathrm{d}\tilde{z} =& \int_0^{\tilde{h}} \tilde{u}\phi\cos\theta\left(-\mu_b + \varepsilon\frac{\tilde{U}^{(1)}}{B\tilde{U}^{(0)}}\right)\mathrm{d}\tilde{z} + \varepsilon\int_0^{\tilde{h}} \tilde{u}^{(0)}\frac{\partial \tilde{\tau}_{xz}^{(1)}}{\partial \tilde{z}}\mathrm{d}\tilde{z} + O(\varepsilon^2)\\ =& \phi\tilde{h}\cos\theta\left[-\tilde{U}\mu_b + \varepsilon\frac{\tilde{U}^{(1)}}{B} + \varepsilon\tilde{A}\frac{\partial \tilde{h}}{\partial \tilde{x}}\left(\frac{2}{5}\tilde{h}^{3/2} - \frac{F^2\tilde{A}^2\tilde{h}^{7/2}}{10\cos\theta}\right)\right] + O(\varepsilon^2).\end{aligned} \tag{A.2}$$

We compute

$$\frac{\tilde{U}^{(1)}}{B} + \tilde{A}\frac{\partial \tilde{h}}{\partial \tilde{x}}\left(\frac{2}{5}\tilde{h}^{3/2} - \frac{F^2\tilde{A}^2}{10\cos\theta}\tilde{h}^{7/2}\right) = \tilde{A}\frac{\partial \tilde{h}}{\partial \tilde{x}}\frac{3C}{10}\tilde{h}^{3/2} \tag{A.3}$$

We thus obtain the following equation for the energy:

$$\begin{aligned}&\frac{\partial}{\partial \tilde{t}}\left(\tilde{h}\frac{\tilde{U}^2}{2} + \frac{\tilde{h^3}\tilde{\psi}}{2} + \frac{\tilde{h}^2\cos\theta}{2F^2}\right) + \frac{\partial}{\partial \tilde{x}}\left(\frac{\tilde{h}\tilde{U}^3}{2} + \frac{3}{2}\tilde{h}^3\tilde{U}\tilde{\psi} + \frac{\tilde{h}^2\tilde{U}}{F^2}\cos\theta\right)\\ &= \frac{\tilde{h}\tilde{U}\cos\theta}{\varepsilon F^2}(\tan\theta - \mu_b) + \frac{\tilde{A}^3\tilde{h}^{9/2}}{125}\frac{\partial \tilde{h}}{\partial \tilde{x}} + \frac{3}{10}\tilde{A}C\tilde{h}^{5/2}\frac{\cos\theta}{F^2}\frac{\partial \tilde{h}}{\partial \tilde{x}} + O(\varepsilon).\end{aligned} \tag{A.4}$$

To ensure compatibility between the energy equation and the momentum equation, we need to modify the left-hand side of (A.4). We compute with (4.3), (4.8) and (4.13)

$$\frac{1}{2}\frac{\partial \tilde{h^3}\tilde{\psi}}{\partial \tilde{t}} + \frac{3}{2}\frac{\partial \tilde{h^3}\tilde{U}\tilde{\psi}}{\partial \tilde{x}} = \frac{13}{250}\tilde{A}^3\tilde{h}^{9/2}\frac{\partial \tilde{h}}{\partial \tilde{x}} + O(\varepsilon). \tag{A.5}$$

Similarly,

$$C\left(\frac{3}{4} - \frac{\lambda}{7}\right)\left(\frac{\partial}{\partial \tilde{t}}\frac{\tilde{h}^2\cos\theta}{2F^2} + \frac{\partial}{\partial \tilde{x}}\frac{\tilde{h}^2\tilde{U}\cos\theta}{F^2}\right) = \frac{2C}{5}\left(\frac{3}{4} - \frac{\lambda}{7}\right)\tilde{A}\tilde{h}^{5/2}\frac{\cos\theta}{F^2}\frac{\partial \tilde{h}}{\partial \tilde{x}} + O(\varepsilon). \tag{A.6}$$

We now subtract Equations $(1-\beta)$(A.5) + (A.6) from (A.4) to obtain

$$\begin{aligned}&\frac{\partial}{\partial \tilde{t}}\left(\tilde{h}\frac{\tilde{U}^2}{2} + \frac{\beta\tilde{h^3}\tilde{\psi}}{2} + K\frac{\tilde{h}^2\cos\theta}{2F^2}\right) + \frac{\partial}{\partial \tilde{x}}\left(\frac{\tilde{h}\tilde{U}^3}{2} + \frac{3\beta\tilde{h}^3\tilde{U}\tilde{\psi}}{2} + K\frac{\tilde{h}^2\tilde{U}\cos\theta}{F^2}\right)\\ =&\frac{\tilde{h}\tilde{U}\cos\theta}{\varepsilon F^2}(\tan\theta - \mu_b) + \frac{13\beta - 11}{250}\tilde{A}^3\tilde{h}^{9/2}\frac{\partial \tilde{h}}{\partial \tilde{x}} + \frac{2\lambda}{35}\tilde{A}C\tilde{h}^{5/2}\frac{\cos\theta}{F^2}\frac{\partial \tilde{h}}{\partial \tilde{x}} + O(\varepsilon).\end{aligned} \tag{A.7}$$

We recognize the work associated to the basal friction in the first term of the right-hand side. We still need to find a suitable expression for the remaining terms. First, it follows from the definition of β (4.28), the expression of $\tilde{U}^{(0)}$ (4.3) and Equation (4.12) that

$$\begin{aligned}&\frac{13\beta - 11}{250}\tilde{A}^3\tilde{h}^{9/2}\frac{\partial \tilde{h}}{\partial \tilde{x}} + \frac{2\lambda}{35}\frac{\cos\theta}{F^2}\tilde{A}\frac{\partial \tilde{h}}{\partial \tilde{x}}\tilde{h}^{5/2}\\ =&-\frac{3\beta}{250}\tilde{A}^3\tilde{h}^{9/2}\frac{\partial \tilde{h}}{\partial \tilde{x}} + \lambda\frac{10}{\tilde{A}^2B}\frac{\cos\theta}{F^2}\tilde{U}^{(0)}\frac{\partial \tilde{h}}{\partial \tilde{x}}\left(\tilde{\psi}^{(1)} - \frac{\tilde{A}\tilde{U}^{(1)}}{5\tilde{h}^{1/2}}\right).\end{aligned} \tag{A.8}$$

By using equations (4.3), (4.7) and (4.12), we get the following exact equality:

$$-\frac{3}{250}\tilde{A}^3\tilde{h}^{9/2}\frac{\partial \tilde{h}}{\partial \tilde{x}} = \frac{\cos\theta}{F^2}\tilde{U}^{(0)}\left(\frac{\tilde{\alpha}_1(\theta)}{\tilde{h}^{1/2}}\tilde{U}^{(1)} + \tilde{\alpha}_2(\theta)\left(\tilde{\psi}^{(1)} - \frac{\tilde{A}\tilde{U}^{(1)}}{5\tilde{h}^{1/2}}\right)\right), \tag{A.9}$$

where

$$\alpha_1(\theta) = -\frac{33C}{2AB(34C+28)}, \qquad \tilde{\alpha}_1(\theta) = -\frac{33C}{2\tilde{A}B(34C+28)}, \tag{A.10}$$

and

$$\alpha_2(\theta) = \frac{77(9C-12)}{2A^2B(34C+28)}, \qquad \tilde{\alpha}_2(\theta) = \frac{77(9C-12)}{2\tilde{A}^2B(34C+28)}. \tag{A.11}$$

Recall that $\tilde{U}^{(0)} = \tilde{U} + O(\varepsilon)$. Similarly, equation (4.2) can be written

$$\tilde{U}^{(1)} = \frac{\tilde{U}-\tilde{U}^{(0)}}{\varepsilon} + O(\varepsilon) = \frac{1}{\varepsilon}\left(\tilde{U} - \frac{2}{5}\tilde{A}\tilde{h}^{3/2}\right) + O(\varepsilon), \tag{A.12}$$

and similarly for (4.11)

$$\tilde{\psi}^{(1)} - \frac{\tilde{A}\tilde{U}^{(1)}}{5\tilde{h}^{1/2}} = \frac{1}{\varepsilon}\left(\tilde{\psi} - \frac{\tilde{U}^2}{4\tilde{h}^2}\right) + O(\varepsilon). \tag{A.13}$$

We can thus modify (A.9) and obtain

$$-\frac{3}{250}\tilde{A}^3\tilde{h}^{9/2}\frac{\partial \tilde{h}}{\partial \tilde{x}} = \frac{\tilde{U}\cos\theta}{\varepsilon F^2}\left[\frac{\tilde{\alpha}_1(\theta)}{\tilde{h}^{1/2}}\left(\tilde{U} - \frac{2}{5}\tilde{A}\tilde{h}^{3/2}\right) + \tilde{\alpha}_2(\theta)\left(\tilde{\psi} - \frac{\tilde{U}^2}{4\tilde{h}^2}\right)\right] + O(\varepsilon). \tag{A.14}$$

In a similar fashion, we have

$$\lambda\frac{10}{\tilde{A}^2B}\frac{\cos\theta}{F^2}\tilde{U}^{(0)}\frac{\partial \tilde{h}}{\partial \tilde{x}}\left(\tilde{\psi}^{(1)} - \frac{\tilde{A}\tilde{U}^{(1)}}{5\tilde{h}^{1/2}}\right) = \lambda\tilde{U}\frac{10\cos\theta}{\varepsilon F^2\tilde{A}^2B}\left(\tilde{\psi} - \frac{\tilde{U}^2}{4\tilde{h}^2}\right) + O(\varepsilon). \tag{A.15}$$

Appendix B. Diffusive terms in the energy balance equation

Equation (3.13) yields

$$\tilde{u}^{(0)}\frac{\partial \tilde{\tau}_{xx}^{(0)}}{\partial \tilde{x}} = \frac{2\tilde{A}}{3}\left(\tilde{h}^{3/2} - (\tilde{h}-\tilde{z})^{3/2}\right)\frac{\partial \tilde{\tau}_{xx}^{(0)}}{\partial \tilde{x}}. \tag{B.1}$$

From previous computations, we obtain

$$\int_0^{\tilde{h}} \tilde{h}^{3/2}\frac{\partial \tilde{\tau}_{xx}^{(0)}}{\partial \tilde{x}} = \frac{2}{3}\phi\sin\theta\left[\left(\frac{\partial \tilde{h}}{\partial \tilde{x}}\right)^2\tilde{h}^{5/2} + \frac{\partial^2\tilde{h}}{\partial \tilde{x}}\frac{\tilde{h}^{7/2}}{2}\right] \tag{B.2}$$

We also compute with (5.28)

$$\int_0^{\tilde{h}} (\tilde{h}-\tilde{z})^{3/2}\frac{\partial \tilde{\tau}_{xx}^{(0)}}{\partial \tilde{x}} = \frac{2}{3}\phi\sin\theta\left[\left(\frac{\partial \tilde{h}}{\partial \tilde{x}}\right)^2\frac{\tilde{h}^{5/2}}{20} + \frac{\partial^2\tilde{h}}{\partial \tilde{x}^2}\frac{\tilde{h}^{7/2}}{7}\right] \tag{B.3}$$

Hence

$$\int_0^{\tilde{h}} \tilde{u}^{(0)}\frac{\partial \tilde{\tau}_{xx}^{(0)}}{\partial \tilde{x}} = \frac{2}{9}\tilde{A}\phi\sin\theta\left[\left(\frac{\partial \tilde{h}}{\partial \tilde{x}}\right)^2\frac{19}{10}\tilde{h}^{5/2} + \frac{\partial^2\tilde{h}}{\partial \tilde{x}^2}\frac{5}{7}\tilde{h}^{7/2}\right] \tag{B.4}$$

and

$$\begin{aligned}\int_0^{\tilde{h}} \tilde{u}^{(0)}\frac{\partial \tilde{\tau}_{xx}^{(0)}}{\partial \tilde{x}} - \phi F^2\frac{\partial}{\partial \tilde{x}}\left(\tilde{\nu}_{\text{eff}}\tilde{h}\tilde{U}^{(0)}\frac{\partial \tilde{U}^{(0)}}{\partial \tilde{x}}\right) &= \frac{2\tilde{A}\phi\sin\theta}{3}\left[-\frac{1}{15}\tilde{h}^{5/2}\left(\frac{\partial \tilde{h}}{\partial \tilde{x}}\right)^2 + \frac{4}{105}\tilde{h}^{7/2}\frac{\partial^2\tilde{h}}{\partial \tilde{x}^2}\right] \\ &= \phi F^2\left[\frac{8}{7}\frac{\partial}{\partial \tilde{x}}\left(\tilde{\nu}_{\text{eff}}\tilde{h}^3\frac{\partial \tilde{\psi}^{(0)}}{\partial \tilde{x}}\right) - \frac{2}{3}\tilde{\nu}_{\text{eff}}\tilde{h}\left(\frac{\partial \tilde{U}^{(0)}}{\partial \tilde{x}}\right)^2\right].\end{aligned} \tag{B.5}$$

References

B. Andreotti, Y. Forterre, and O. Pouliquen. *Granular Media, Between Fluid and Solid*. Cambridge University Press, 2013. doi: 10.1017/CBO9780511840531.

T. Börzsönyi and R. E. Ecke. Rapid granular flows on a rough incline: Phase diagram, gas transition, and effects of air drag. *Physical Review E*, 74(6):061301, 2006.

D. Denisenko, G. L. Richard, and G. Chambon. A consistent three-equation shallow-flow model for Bingham fluids. *Journal of Non-Newtonian Fluid Mechanics*, 321:105111, 2023.

Y. Forterre. Kapiza waves as a test for three-dimensional granular flow rheology. *Journal of Fluid Mechanics*, 563:123–132, 2006. doi: 10.1017/S0022112006001509.

Y. Forterre and O. Pouliquen. Long-surface-wave instability in dense granular flows. *Journal of Fluid Mechanics*, 486:21–50, 2003. doi: 10.1017/S0022112003004555.

GDR MiDi. On dense granular flows. *The European Physical Journal E*, 14:341–365, 2004.

J. Gray and A. Edwards. A depth-averaged $\mu(I)$-rheology for shallow granular free-surface flows. *Journal of Fluid Mechanics*, 755:297–329, 09 2014. doi: 10.1017/jfm.2014.450.

P. Jop, Y. Forterre, and O. Pouliquen. Crucial role of sidewalls in granular surface flows: consequences for the rheology. *Journal of fluid mechanics*, 541:167–192, 2005.

P. Jop, Y. Forterre, and O. Pouliquen. A constitutive law for dense granular flows. *Nature*, 441(7094):727–730, 2006.

A. Mangeney, F. Bouchut, N. Thomas, J.-P. Vilotte, and M.-O. Bristeau. Numerical modeling of self-channeling granular flows and of their levee-channel deposits. *Journal of Geophysical Research: Earth Surface*, 112(F2), 2007.

A. Mangeney-Castelnau, J.-P. Vilotte, M.-O. Bristeau, B. Perthame, F. Bouchut, C. Simeoni, and S. Yerneni. Numerical modeling of avalanches based on Saint-Venant equations using a kinetic scheme. *Journal of Geophysical Research: Solid Earth*, 108(B11), 2003.

A. Mangeney-Castelnau, F. Bouchut, J.-P. Vilotte, E. Lajeunesse, A. Aubertin, and M. Pirulli. On the use of Saint-Venant equations to simulate the spreading of a granular mass. *Journal of Geophysical Research: Solid Earth*, 110(B9), 2005.

O. Pouliquen. Scaling laws in granular flows down rough inclined planes. *Physics of fluids*, 11(3):542–548, 1999.

O. Pouliquen and Y. Forterre. Friction law for dense granular flows: application to the motion of a mass down a rough inclined plane. *Journal of fluid mechanics*, 453:133–151, 2002.

O. Pouliquen, C. Cassar, Y. Forterre, P. Jop, and M. Nicolas. How do grains flow: towards a simple rheology for dense granular flows. *Powders and Grains*, pages 859–865, 2005.

G. L. Richard. Roll waves in a predictive model for open-channel flows in the smooth turbulent case. *Journal of Fluid Mechanics*, 983:A31, 2024.

G. L. Richard and S. L. Gavrilyuk. A new model of roll waves: comparison with Brock's experiments. *Journal of Fluid Mechanics*, 698:374–405, 2012.

G. L. Richard, C. Ruyer-Quil, and J.-P. Vila. A three-equation model for thin films down an inclined plane. *Journal of Fluid Mechanics*, 804:162–200, 2016.

C. Ruyer-Quil and P. Manneville. Improved modeling of flows down inclined planes. *The European Physical Journal B-Condensed Matter and Complex Systems*, 15: 357–369, 2000.

S. B. Savage and K. Hutter. The motion of a finite mass of granular material down a rough incline. *Journal of fluid mechanics*, 199:177–215, 1989.

V. M. Teshukov. Gas-dynamic analogy for vortex free-boundary flows. *Journal of Applied Mechanics and Technical Physics*, 48:303–309, 2007.

[1]Aix Marseille Univ., CNRS, Centrale Marseille, I2M UMR CNRS 7373, 13000 Marseille, France

[2]Univ. Grenoble Alpes, CNRS, INRAE, IRD, Grenoble INP, IGE, 38000 Grenoble, France

Email address: gael.richard@inrae.fr